Report Documentation Page

Form Approved
OMB No. 0704-0188

Public reporting burden for the collection of information is estimated to average 1 hour per response, including the time for reviewing instructions, searching existing data sources, gathering and maintaining the data needed, and completing and reviewing the collection of information. Send comments regarding this burden estimate or any other aspect of this collection of information, including suggestions for reducing this burden, to Washington Headquarters Services, Directorate for Information Operations and Reports, 1215 Jefferson Davis Highway, Suite 1204, Arlington VA 22202-4302. Respondents should be aware that notwithstanding any other provision of law, no person shall be subject to a penalty for failing to comply with a collection of information if it does not display a currently valid OMB control number.

1. REPORT DATE **JUN 2002**	2. REPORT TYPE	3. DATES COVERED **00-00-2002 to 00-00-2002**
4. TITLE AND SUBTITLE **Simulations of the quasi-biennial oscillation and its effect on stratospheric H2O, CH4, and age of air with an interactive two-dimensional model**		5a. CONTRACT NUMBER 5b. GRANT NUMBER 5c. PROGRAM ELEMENT NUMBER
6. AUTHOR(S)		5d. PROJECT NUMBER 5e. TASK NUMBER 5f. WORK UNIT NUMBER
7. PERFORMING ORGANIZATION NAME(S) AND ADDRESS(ES) **Naval Research Laboratory,E. O. Hulburt Center for Space Research,Washington,DC,20375**		8. PERFORMING ORGANIZATION REPORT NUMBER
9. SPONSORING/MONITORING AGENCY NAME(S) AND ADDRESS(ES)		10. SPONSOR/MONITOR'S ACRONYM(S) 11. SPONSOR/MONITOR'S REPORT NUMBER(S)
12. DISTRIBUTION/AVAILABILITY STATEMENT **Approved for public release; distribution unlimited**		
13. SUPPLEMENTARY NOTES		
14. ABSTRACT		
15. SUBJECT TERMS		

16. SECURITY CLASSIFICATION OF:			17. LIMITATION OF ABSTRACT	18. NUMBER OF PAGES	19a. NAME OF RESPONSIBLE PERSON
a. REPORT **unclassified**	b. ABSTRACT **unclassified**	c. THIS PAGE **unclassified**	**Same as Report (SAR)**	**17**	

Standard Form 298 (Rev. 8-98)
Prescribed by ANSI Std Z39-18

Simulations of the quasi-biennial oscillation and its effect on stratospheric H_2O, CH_4, and age of air with an interactive two-dimensional model

J. P. McCormack and D. E. Siskind

E. O. Hulburt Center for Space Research, Naval Research Laboratory, Washington, District of Columbia, USA

Received 28 January 2002; revised 20 June 2002; accepted 24 June 2002; published 20 November 2002.

[1] A zonally averaged photochemical–dynamical model of the middle atmosphere is used to simulate the quasi-biennial oscillation (QBO) and its effect on the distributions of stratospheric H_2O, CH_4, and age of air. Changes in planetary wave amplitudes of ±25% cause 2–3 month changes in QBO period. Comparable changes in prescribed tropical heating have a smaller effect on the QBO period. The response of tropical upwelling, and QBO period, to changes in extratropical forcing depends on the magnitude and location of the imposed changes. In the Southern Hemisphere, where the planetary wave forcing is smaller than in the Northern Hemisphere, increased forcing produces stronger equatorial upwelling and a longer QBO period. In the Northern Hemisphere, increased forcing produces weaker upwelling and a shorter QBO period due to the larger amplitude waves becoming saturated. Overall, the effect of the QBO is to produce a slightly younger mean age of air near the tropical stratopause due to the model not exactly reproducing the strength and duration of the observed westerly wind shear. The QBO in lower stratospheric H_2O, but not CH_4, results primarily from meridional circulation anomalies superimposed upon background gradients in H_2O mixing ratio that are maintained by the annual cycle in lower stratospheric H_2O. QBO modulation of horizontal eddy transport plays a much smaller role. A realistic annual cycle in equatorial H_2O mixing ratio at the model tropopause produces a QBO variation in lower stratospheric H_2O of 0.1–0.2 ppmv. The effect of the QBO on model tropical tropopause temperatures doubles the amplitude of the water vapor QBO at 20 km. *INDEX TERMS:* 0341 Atmospheric Composition and Structure: Middle atmosphere—constituent transport and chemistry (3334); 3334 Meteorology and Atmospheric Dynamics: Middle atmosphere dynamics (0341, 0342); 3374 Meteorology and Atmospheric Dynamics: Tropical meteorology; *KEYWORDS:* QBO, water, vapor, methane, stratosphere

Citation: McCormack, J. P., and D. E. Siskind, Simulations of the quasi-biennial oscillation and its effect on stratospheric H_2O, CH_4, and age of air with an interactive two-dimensional model, *J. Geophys. Res.*, *107*(D22), 4625, doi:10.1029/2002JD002141, 2002.

1. Introduction

[2] Interannual variability in tropical stratospheric ascent is dominated by circulation anomalies associated with the quasi-biennial oscillation (QBO) in equatorial zonal winds. The QBO consists of alternating easterlies and westerlies that first appear in the equatorial upper stratosphere and descend at a rate of approximately 1 km month^{-1} (for a comprehensive review of QBO observations and theory, see the work of *Baldwin et al.* [2001]). During periods of westerly (easterly) shear, a pattern of anomalous vertical motion is established consisting of weaker (stronger) ascent over the equator and stronger (weaker) ascent over the subtropics [*Reed*, 1964]. The resulting downward (upward) anomalies in the ascent rates produce warm (cold) temperature anomalies to maintain a cross-equatorial temperature gradient that is in thermal wind balance with the zonal wind shear [e.g., *Andrews et al.*, 1987]. This QBO-induced circulation then alters the latitude/height distributions of long-lived stratospheric constituents such as H_2O, CH_4, odd nitrogen compounds, and O_3. The goal of this paper is to describe the effects of the QBO on the stratospheric distributions of H_2O, CH_4, and age of air using an interactive zonally averaged photochemical–dynamical model.

[3] Previous modeling studies of QBO variability in stratospheric constituents have highlighted the interaction between the annually varying mean meridional circulation and the QBO-induced circulation anomalies. For example, *Gray and Pyle* [1989] successfully reproduced many of the QBO-related features observed in global satellite-based total ozone column records using a self-consistent (i.e., not imposed) QBO in equatorial zonal winds. These features include the phase reversal of the total ozone QBO between the equatorial and subtropical regions, the synchronization of the extratropical signal with the seasonal cycle, and the hemispheric asymmetry in the high latitude total ozone QBO. The latter two features arise from a nonlinear inter-

This paper is not subject to U.S. copyright.
Published in 2002 by the American Geophysical Union.

action between the QBO-induced circulation and the seasonally varying mean meridional circulation [*Gray and Dunkerton*, 1990]. *Jones et al.* [1998] showed that the resulting asymmetric pattern of vertical and horizontal momentum advection in the tropics is strongest in the winter hemisphere and is sufficient to explain the observed extratropical QBO in total ozone. *Jones et al.* [1998] also showed that QBO-related circulation anomalies can modify the spatial gradients of long-lived trace gases in the tropical stratosphere, which in turn affect the transport of these constituents to the extratropics through mixing by breaking planetary waves.

[4] The two primary sources of H_2O throughout the middle atmosphere (15–100 km altitude) are chemical production at higher altitudes by methane oxidation and transport of water vapor across the tropical tropopause [e.g., *Summers et al.*, 1997]. The amount of H_2O transported across the tropical tropopause is dependent on both the strength of the upward motion and the temperature distribution in that region. *Bacmeister et al.* [1998] showed that annual mean ascent rates in the tropical stratosphere above 20 km can be sensitive to changes in the strength of a prescribed latent heat source and to changes in the amplitude of extratropical planetary wave forcing. Because adiabatic cooling associated with ascent controls the variations in tropical lower stratospheric temperatures [*Yulaeva et al.*, 1994; *Holton et al.*, 1995], the strength of upward motion influences the saturation mixing ratio of air parcels entering the lower stratosphere, producing the well-known "tape recorder" effect [*Mote et al.*, 1996]. The study of *Summers et al.* [1997] used a fixed lower boundary value for H_2O, so the sensitivity of the lower stratospheric water vapor budget to varying ascent rates could not be determined. More recently, *Gettleman et al.* [2000] carried out simulations of water vapor exchange across the tropical tropopause using a three-dimensional chemical tracer model that was able to reproduce the tape recorder effect in a qualitative sense using prescribed winds and temperatures. How the stratospheric H_2O distribution responds to changes in transport and temperature related to the QBO in an interactive model simulation remains an open question.

[5] An analysis of HALOE H_2O and CH_4 measurements by *Randel et al.* [1998] confirms that the distributions of these long-lived constituents are influenced by QBO-induced circulation anomalies [e.g., *Randel et al.*, 1999]. Above 30 km, the H_2O and CH_4 anomalies are opposite in sign to one another, which is consistent with the fact that H_2O increases with height and CH_4 decreases with height throughout the middle atmosphere. Below 30 km, however, there is evidence of a QBO signal in equatorial water vapor in the lower stratosphere but no evidence of a methane QBO [*Randel et al.*, 1998; *Baldwin et al.*, 2001]. This suggests a dynamical origin for the water vapor QBO anomaly in the lower stratosphere involving processes that control the transport of water vapor across the tropical tropopause [*Dunkerton*, 2001]. While these observations indicate a clear QBO signal in water vapor throughout the equatorial stratosphere, the data records are not of sufficient length to investigate long-term (i.e., decadal) variability in stratospheric water vapor and methane arising from interactions between the QBO and the annual cycle, similar to what has been observed in the total ozone records.

[6] In the present work, we use an updated version of a zonally averaged two-dimensional photochemical–dynamical model of the middle atmosphere, CHEM2D, to quantify the effect of the QBO on water vapor, methane, and the age of air in the middle atmosphere. The latest version of CHEM2D contains two important new features designed to simulate more realistic interannual variability in the transport of long-lived trace constituents such as O_3, H_2O, and CH_4. These features include an interactive (i.e., not imposed) parameterization for the QBO and an annually varying source of lower stratospheric H_2O that is consistent with modeled tropical tropopause temperatures (i.e., the tape recorder effect). Using this approach, we first evaluate the sensitivity of the zonal wind QBO to other processes controlling tropical ascent rates (namely, the strength of extratropical planetary wave forcing and localized tropical heating), and then examine the interannual variability in stratospheric H_2O and CH_4 arising from interactions between the QBO and the seasonal cycle in tropical tropopause temperatures.

[7] The paper is organized as follows: section 2 describes the current model formulation; section 3 examines the sensitivity of the modeled QBO to changes in the strength of planetary wave activity and diabatic heating, the effect of the QBO on age of air estimates, and the low-frequency variability in stratospheric constituents resulting from the interaction between the QBO and the annual cycle; section 4 examines the QBO in the model H_2O and CH_4 distributions and its relationship with the annual cycle in water vapor at the tropical tropopause; section 5 summarizes these results and discusses further applications of this model for studying the long-term evolution of tracer transport in the middle atmosphere.

2. CHEM2D Model Description

[8] The zonally averaged CHEM2D model features a self-consistent treatment of radiative, photochemical, and dynamical processes in the middle atmosphere [e.g., *Bacmeister et al.*, 1995, 1998; *Summers et al.*, 1997; *Siskind et al.*, 1997]. The model grid points are spaced every 4.8° in latitude from pole to pole, with 41 levels in the vertical between the model surface (p = 1000 hPa) and the model top ($p = 2 \times 10^{-4}$ hPa or ~106 km altitude) spaced every 2.6 km. Radiative calculations are performed once per day, and the model dynamics are updated every 2 hours. This section highlights several features of the model dynamics that are relevant for constituent transport by the mean meridional circulation. *Siskind et al.* [2000] reviews the updated chemistry and advection schemes in the current version of the model. The most recent version of CHEM2D has an improved parameterization for gravity wave drag by zero phase speed waves [*Siskind et al.*, in review, 2002].

[9] Zonal mean winds from a 20 year reference simulation are shown in Figure 1 for the months of January and July. The model captures several important dynamical features including the wintertime zonal wind profile in the midlatitude stratosphere and the differing strengths of the polar jets between the two hemispheres. One feature of earlier CHEM2D simulations of the middle atmosphere is the persistence of the polar vortex past late winter and well into spring. This is a result of insufficient gravity wave drag

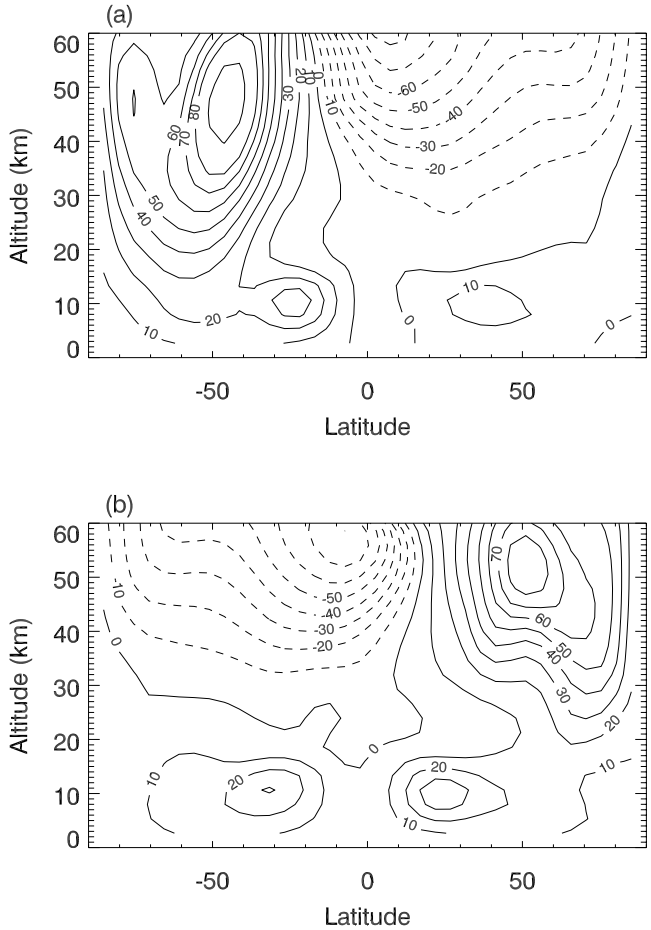

Figure 1. Latitude–height cross sections of zonal wind in (a) January and (b) July from model experiment *Q*0 (see Table 1).

leading to reduced descent and adiabatic heating within the polar vortex. In the past, this problem has been corrected by imposing arbitrary sources of wave-induced drag. The gravity wave drag parameterization in the latest version of the CHEM2D model reduces, but does not completely eliminate, the problem. Since the vertical velocity field in the equatorial lower stratosphere is sensitive to imposed wave drag through nonlocal forcing of the meridional circulation, ad hoc corrections can introduce unwanted irregularities in the modeled descent of alternating phases of the QBO. To avoid these irregularities, the present version of CHEM2D does not arbitrarily increase planetary wave amplitudes every spring to force a final warming of the polar vortex.

[10] Several past observational and modeling studies have suggested a coupling between the semiannual oscillation (SAO) in equatorial zonal winds and the QBO. For example, *Gray and Pyle* [1989] demonstrated that the maximum westerly acceleration of the modeled zonal wind QBO appears during periods of SAO westerlies. Furthermore, there is evidence that the easterly phase of the mesospheric SAO is stronger during the stratospheric QBO westerly phase [*Burrage et al.*, 1996; *Garcia et al.*, 1997], giving rise to an apparent mesospheric QBO. Both past and present versions of CHEM2D generate a weak semiannual oscillation (SAO) in equatorial zonal winds between 45 and 80 km due to advection of easterly momentum by the seasonally varying meridional circulation [*Summers et al.*, 1997]. This "spontaneous" SAO does not produce the annual mean westerly flow that is observed between 60 and 80 km [*Garcia et al.*, 1997], which indicates that the model lacks an appropriate source of westerly (or eastward) momentum. A realistic SAO in equatorial zonal wind can be produced with the inclusion of additional equatorial gravity wave modes [see *Garcia et al.*, 1992]. However, because the present work focuses solely on the dynamical and transport effects of the QBO, the model does not include any explicit SAO parameterization. Interactions between the QBO and SAO in the CHEM2D model will be the subject of a future study.

2.1. Mechanical and Thermodynamic Forcing

[11] The dynamical framework of the model is based on the Transformed Eulerian Mean (TEM) formulation, in which the residual meridional circulation is driven by zonally averaged sources of momentum and thermodynamic forcing [*Andrews et al.*, 1987]. This circulation is determined by combining the zonally averaged angular momentum and thermodynamic equations, subject to the constraint of thermal wind balance, to form a diagnostic relation for the meridional stream function in terms of the total mechanical forcing $\mathcal{X}$ and the total thermodynamic forcing $\mathcal{H}$, where

$$\mathcal{X} = D_{GW} + \nabla \cdot \mathbf{F}_{PW} - \alpha_{Ray}\bar{u} + \frac{\partial}{\partial z}\left(K_{mom}\frac{\partial}{\partial z}\bar{u}\right) \qquad (1)$$

$$\mathcal{H} = \mathcal{H}_{rad} + \mathcal{H}_{LH} - \alpha_{bdy}\left(\bar{\theta} - \bar{\theta}_{NCEP}\right) + \frac{\partial}{\partial z}\left(K_{therm}\frac{\partial}{\partial z}\bar{\theta}\right). \qquad (2)$$

The different components of the total forcing $\mathcal{X}$ and $\mathcal{H}$ are described below; details of the individual components are discussed by *Bacmeister et al.* [1998].

[12] The total mechanical forcing $\mathcal{X}$ consists of a gravity wave drag (D_{GW}) parameterization for both stationary and nonzero phase speed gravity waves, the Eliassen–Palm (EP) flux divergence associated with dissipating or breaking planetary waves, drag due to Rayleigh friction (which becomes significant at altitudes above 50 km), and vertical mixing of momentum by gravity wave breaking and molecular diffusion represented by the term K_{mom} (important in the upper mesosphere). As mentioned in the Introduction, it is the action of extratropical planetary waves through the EP flux divergence term that drives the seasonally varying meridional circulation and controls the annual temperature cycle above the tropical tropopause. The contribution to $\mathcal{X}$ from the EP flux divergence is determined through solution of a linear, time-dependent, three-dimensional planetary wave model using model winds and temperatures. Horizontal mixing associated with planetary wave breaking is estimated using an extension of the *Garcia* [1991] parameterization [*Bacmeister et al.*, 1995]. Currently, the model generates solutions for a fixed-amplitude zonal wave number 1 disturbance at the lower boundary. The amplitude of this boundary condition varies with latitude but remains constant throughout the year.

[13] The thermodynamic forcing $\mathcal{H}$ consists of the net radiative heating rate $\mathcal{H}_{rad}$, prescribed tropospheric heating $\mathcal{H}_{LH}$ representing latent heat released by convective activity that is not explicitly included in the model, the estimated

lower atmospheric heating and cooling by surface processes derived from National Centers for Environmental Prediction (NCEP) climatological temperature analyses, and eddy diffusion of heat (K_{therm}) by breaking gravity waves in the mesosphere. The net radiative heating rate $\mathcal{H}_{rad}$ is determined by merging the results of two different radiative transfer schemes for the altitude region below 20 km [*Rosenfield et al.*, 1987] and the region above 20 km [*Zhu et al.*, 1992]. Unlike earlier studies [e.g., *Summers et al.*, 1997], shortwave heating and longwave cooling rates above 20 km are determined using model temperature and constituent fields, allowing for interaction between radiative and transport processes in this region. The prescribed latent heating $\mathcal{H}_{LH}$, as a function of latitude and altitude, is taken from monthly mean climatological precipitation estimates (K. Rosenlof, private communication, 1997). This differs from the analytic form used previously by *Bacmeister et al.* [1998]. For the coupled simulations presented here, all values of the latent heating have been scaled by a factor of 0.5 to make the modeled age of air in the stratosphere (see section 3.1) agree better with observations [*Hall and Plumb*, 1994].

2.2. Parameterization of the QBO

[14] The inclusion of the equatorial zonal wind QBO in CHEM2D follows the theory of *Lindzen and Holton* [1968], who showed that a realistic zonal wind QBO can be generated from the preferential damping of a broad spectrum of upward propagating gravity waves. In the present model, the vertical momentum flux resulting from the radiative damping of easterly and westerly equatorial wave modes can be parameterized in terms of the tropospheric forcing (F), phase speed (c), and model profiles of the equatorial zonal wind ($\bar{u}$), buoyancy frequency (N), and the radiative damping rate (α) [*Holton and Lindzen*, 1972]. Although it has long been recognized that a broad spectrum of gravity waves must provide the momentum flux necessary to generate the observed QBO, numerous one-dimensional and two-dimensional simulations have produced a realistic QBO using a single Kelvin wave mode as a source of westerly momentum and a single Rossby-gravity wave mode as a source of easterly momentum [see *Baldwin et al.*, 2001, and references therein].

[15] Using the formulation of *Dunkerton* [1979], we add an additional component to the zonally averaged mechanical forcing $\mathcal{X}$ of the elliptical stream function equation (1) representing the QBO forcing:

$$\begin{aligned} X_{QBO} &= F_i \exp\left[\frac{z-z_o}{H}\right] D_i \exp[-P_i(z)] \\ P_i(z) &= \int_{z_o}^{z} D_i(z')dz' \\ D_1 &= \frac{\alpha N}{k_0(\bar{u}-c_0)^2} \\ D_2 &= \frac{\alpha N}{k_1(\bar{u}-c_1)^2}\left[\frac{\beta}{k_1^2(\bar{u}-c_1)} - 1\right] \end{aligned} \tag{3}$$

where z is log-pressure altitude, z_o = 17 km is the lower boundary of the parameterization, F_i represents a constant vertical momentum flux at z_o, $\bar{u}$ is the equatorial zonal wind at level z, c_i is the phase speed, and k_i is the horizontal wave number for the Kelvin and Rossby-gravity wave modes i = 1, 2, respectively. The buoyancy frequency N and the β factor have their usual definitions. The radiative damping rate $\alpha(z)$ is specified according to the "slow" damping profile of *Dunkerton* [1979]. The meridional extent of the parameterized momentum forcing for both Kelvin and Rossby-gravity gravity waves decreases exponentially away from the equator with a characteristic length scale Y_L of the form

$$Y_L = \left(\frac{2N}{\beta|m_i|}\right) \tag{4}$$

where the local vertical wave number m_i for each mode is determined by the dispersion relation for upward propagating waves in the presence of vertical wind shear [*Plumb and Bell*, 1982; *Andrews et al.*, 1987].

[16] For the Kelvin wave mode, F_1 = 12 m^2 s^{-2}, c_1 = 30 m s^{-1}, and k_1 corresponds to zonal wave number 2. For the Rossby-gravity wave mode, F_2 = −18 m^2 s^{-2}, c_2 = −30 m s^{-1}, and k_2 corresponds to zonal wave number 4. The values of the parameters in (equation (3)) were chosen to produce a QBO in lower stratospheric equatorial zonal winds that most closely resembles the observed QBO in terms of amplitude, period, and spatial extent, and are comparable to values adopted in previous modeling studies using the same QBO parameterization [*Gray and Pyle*, 1989; *Jones et al.*, 1998].

[17] Many of these earlier studies used a constant value of the vertical momentum diffusion coefficient K_{zz} on the order of 0.5–1.0 m^2 s^{-1}, which is ~10 times larger than estimates of diffusivity inferred from tracer transport in the tropical lower stratosphere [*Mote et al.*, 1998]. In the present study we adopt a fixed vertical profile of K_{mom} in the tropics that ranges from 0.05 m^2 s^{-1} at 20 km up to 0.20 m^2 s^{-1} at 45 km, similar to the observational estimates of *Mote et al.* [1998]. In models with finer vertical resolution (~100 m), using diffusivity estimates based on observations can produce a permanent westerly jet in the equatorial lower stratosphere, indicating that the momentum diffusivity is too small in this region [*Dunkerton*, 2000]. Because of the relatively coarse vertical resolution of the present model, these excessively large shears were not present making any adjustments to the K_{zz} profile unnecessary.

2.3. Varying Lower Boundary Condition for Water Vapor

[18] The evolution of tracers in CHEM2D is governed by the continuity equation for the mixing ratio μ of a chemical constituent

$$\frac{\partial\mu}{\partial t} = -\bar{v}^*\frac{\partial\mu}{a\partial\phi} - \bar{w}^*\frac{\partial\mu}{\partial z} + (P-L) + \frac{1}{a^2\cos 2\phi}\frac{\partial\left[\cos\phi K_{yy}\frac{\partial\mu}{\partial\phi}\right]}{\partial\phi} + \frac{1}{\rho}\frac{\partial\left[\rho K_{zz}\frac{\partial\mu}{\partial z}\right]}{\partial z} \tag{5}$$

The mixing ratio tendency has contributions from advection by the meridional ($\bar{v}^*$) and vertical ($\bar{w}^*$) components of the residual circulation, the net photochemical production (P) and loss (L), horizontal eddy diffusion using K_{yy}

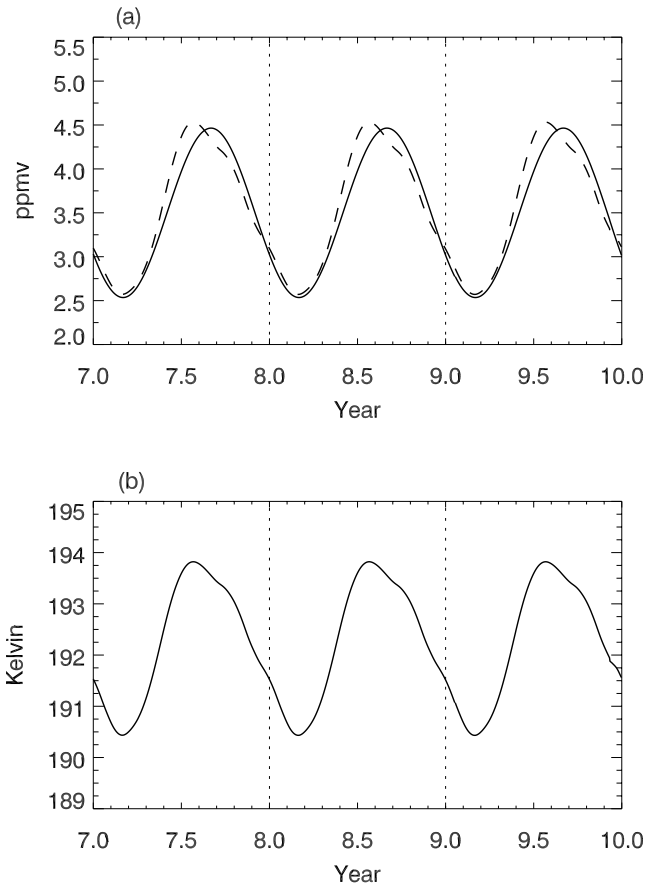

Figure 2. (a) Annual cycle in equatorial H_2O at 15 km using a fixed sinusoidal variation (solid line) and using the modeled annual cycle in temperature −0.5 K (dashed line). (b) Modeled annual cycle in equatorial temperature at 15 km from the $Q0$ experiment used to produce the dashed curve in (a).

from the planetary wave model, and vertical eddy diffusion using $K_{zz} = K_{therm} = P_r^{-1}K_{mom}$ assuming a value of 3 for the Prandtl number P_r [*Summers et al.*, 1997; *Siskind*, 2000].

[19] Earlier versions of CHEM2D specified a constant value of H_2O mixing ratio throughout the model troposphere (i.e., below 15 km). To produce a realistic simulation of stratospheric water vapor transport, it is necessary to account for the seasonal cycle in H_2O mixing ratio in the tropical lower stratosphere. This section describes how this effect is included in the model using two different methods.

[20] The first method is to impose a fixed sinusoidal variation in tropical H_2O mixing ratios at the model tropopause, as in Figure 2a (solid curve). The second method is to allow the model lower boundary condition for water vapor mixing ratios to vary according to the modeled tropical tropopause temperatures using the Clausius–Clapeyron relation. Figure 2b shows the annual cycle in equatorial temperatures at 15 km from a model simulation using standard values of the planetary wave forcing and latent heating with no QBO parameterization (experiment $Q0$ in Table 1). The amplitude of the annual cycle is ∼2 K, which is consistent with observed annual cycle in zonal mean temperatures. However, using the values of the model temperatures themselves produces an annual cycle in H_2O at the tropical tropopause that is much larger than what is observed [e.g., *Randel et al.*, 2001]. This result is not surprising for a zonally averaged model that lacks an explicit treatment of convection and cloud microphysics. We find that by subtracting 0.5 K from the model tropopause temperatures it is possible to produce a "tuned" annual cycle in the tropical H_2O mixing ratios of just over 2 ppmv at 15 km (Figure 2a, dashed curve).

Table 1. QBO Sensitivity Experiments

Experiment	Description	Period (months)
$Q0$	baseline model, no QBO	–
$Q1$	baseline model, with QBO	27
$Q2$	reduced $\mathcal{H}_{LH}$	27
$Q3$	enhanced $\mathcal{H}_{LH}$	28
$Q4$	reduced Z_{NH}	30
$Q5$	enhanced Z_{NH}	24
$Q6$	enhanced Z_{SH}	31

[21] Using either of the two methods listed above to represent the annual cycle in H_2O mixing ratio at the tropical tropopause, CHEM2D is capable of simulating the tape recorder signal in stratospheric H_2O. As Figure 3 shows, regions of alternating moist and dry air propagate upwards at a rate of ∼1 km month^{-1}, similar to observations [*Mote et al.*, 1996]. Although its amplitude is sharply attenuated between 15 and 20 km, the annual cycle is clearly seen up to 30 km altitude. Above 35 km there is evidence of a slight semiannual oscillation, in agreement with the observed seasonal variation of stratospheric water vapor reported by *Randel et al.* [2001].

[22] In its present form, the CHEM2D model is well suited to test the sensitivity of the stratospheric water vapor distribution to a number of different model parameters that govern the ascent rate of air in the tropical lower stratosphere, including (1) changes in the amplitude of planetary wave 1, (2) changes in the magnitude of the

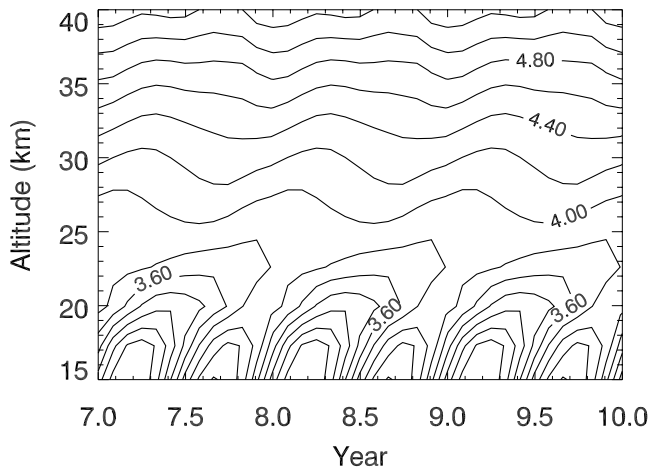

Figure 3. Annual cycle in model stratospheric H_2O at the equator from the $Q0$ simulation using the fixed lower boundary condition. Contour interval is 0.2 ppmv.

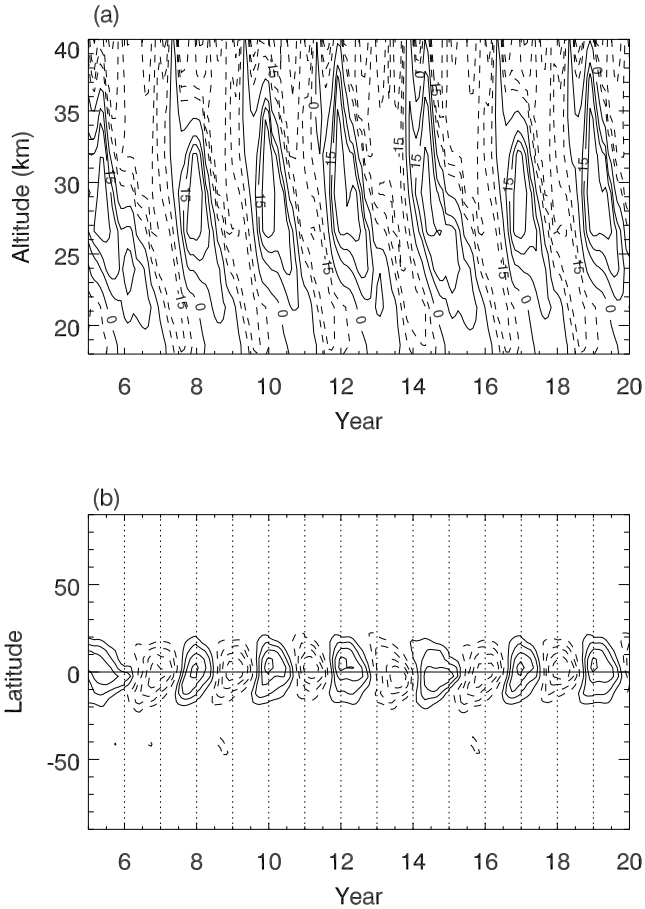

Figure 4. (a) Altitude–time plot of equatorial zonal wind from experiment $Q1$. (b) Corresponding latitude–time section of equatorial zonal wind anomalies (annual cycle removed) at 26 km. Contours drawn at ±5, ±10, ±20, and ±30 m s^{-1}, with dashed contours for negative values.

prescribed latent heating source $\mathcal{H}_{LH}$, and (3) interaction between the QBO and the seasonally varying meridional circulation.

3. Response of the QBO to Changes in External Forcing

[23] This section describes the modeled QBO in zonal mean wind, temperature, and vertical velocity. This section also examines how changes in the dynamical and thermal forcing of the residual meridional circulation affect the QBO. Specifically, we investigate how the period of the modeled QBO varies in response to changes in the imposed planetary wave forcing and prescribed latent heating in the troposphere. Because the extratropical QBO signals in temperature and long-lived constituents are affected by the phasing of the tropical QBO with the seasonal cycle, the interactive model can show how changes in the QBO period modify the interannual variability in the extratropical signals.

3.1. Model QBO in $\bar{u}, \bar{T}, \bar{w}^*$, and Age of Air Estimates

[24] Table 1 lists six different 20 year model simulations (denoted $Q1$–$Q6$), each starting from the same initial conditions, that include the QBO parameterization outlined in section 2.2. Model constituent and dynamical fields are output every 30 days. An additional model run ($Q0$) listed in Table 1 is a reference simulation that is identical to the $Q1$ simulation but does not include the QBO parameterization.

[25] The altitude/time profile of equatorial zonal winds from the $Q1$ simulation in Figure 4a shows alternating westerly and easterly flow between 20 and 35 km with a period of 27 months. The meridional extent of the zonal wind QBO at 26 km (Figure 4b) is ±20° latitude in each hemisphere, which agrees well with observations [*Baldwin et al.*, 2001]. Table 2 gives a detailed comparison of the modeled zonal wind QBO with the observed QBO in Singapore winds (updated from the work of *Naujokat* [1986]). The average value of the peak easterly wind speed at 26 km (~22 hPa) of −21 m s^{-1} is weaker than the corresponding peak easterlies of −33 m s^{-1} in the Singapore record between 1971 and 1997. The average value of maximum westerly shear in the model is 50% less than what is observed. The model does capture the observed asymmetry in the descent rate of the easterly and westerly phases. In general, the modeled westerly phase lasts longer than the easterly phase near 30 km, and vice versa near 20 km, consistent with observations. However, the model does not reproduce the exact altitude at which this transition occurs, so that the duration of the westerly phase at 26 km is longer than the duration of the easterly phase by 1 month, contrary to the observed QBO. It will be shown below that the inaccuracies in the modeled strength and duration of alternating easterly and westerly shear zones can introduce biases in the mean age of air. Nevertheless, the parameterized QBO generates realistic transport anomalies in stratospheric H_2O and CH_4 (see section 4).

[26] A model simulation identical to the $Q1$ run but with the dynamics and radiative heating uncoupled from the photochemistry (not shown) produces similar QBO anomalies in zonal wind, temperature, and residual vertical velocity but with a slightly longer period of 29 months. The shorter QBO period in the coupled simulation is the result of QBO-induced anomalies in lower stratospheric ozone altering the zonal wind QBO through radiative feedback in the lower stratospheric heating rates, similar to the findings of *Cordero and Nathan* [2000]. As with earlier modeling studies using an imposed QBO, [e.g., *Li et al.*, 1995; *Huang*, 1996], we find that radiative feedback of the ozone anomalies has little effect on the amplitude of the zonal wind QBO.

Table 2. Modeled QBO versus Singapore Winds

	CHEM2D	Singapore
$\bar{u}_{max}$ (m s^{-1})[a]	23	20
$\bar{u}_{min}$ (m s^{-1})[a]	−21	−36
$[\frac{\partial \bar{u}}{\partial z}]_{max}$ (m s^{-1} km^{-1})[b]	4.0	8.2
$[\frac{\partial \bar{u}}{\partial z}]_{min}$ (m s^{-1} km^{-1})[b]	−5.6	−6.9
W length (months)[a]	14	12
E length (months)[a]	13	16
W descent (km month^{-1})[c]	1.0	1.4
E descent (km month^{-1})[c]	0.8	0.8

[a] 26 km (~20 hPa).
[b] Centered difference at 26 km.
[c] From 29 to 21 km, ~15–50 hPa.

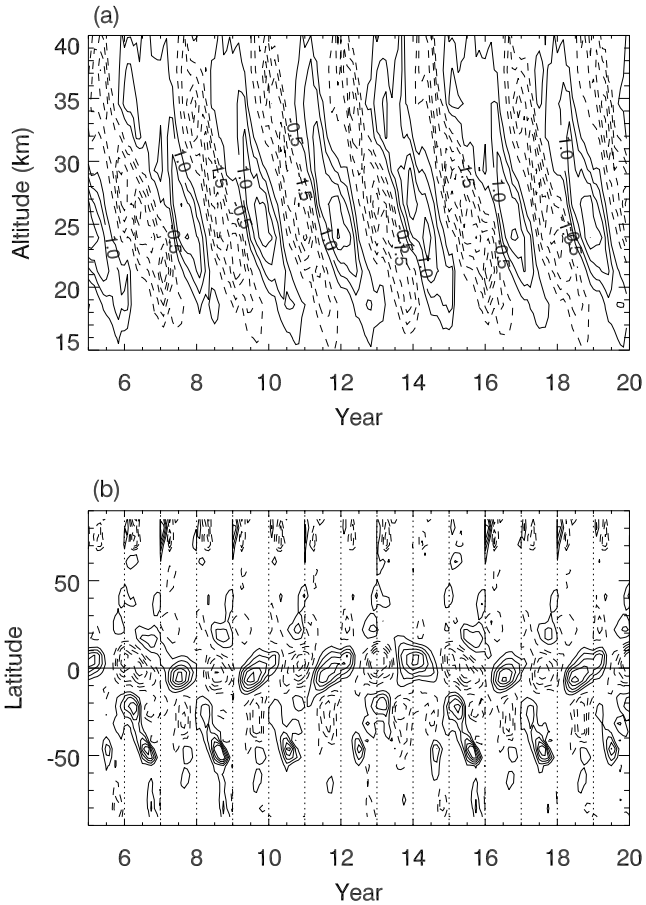

Figure 5. (a) Altitude–time plot of zonal mean temperature anomalies at the equator and (b) temperature anomalies at 26 km from the *Q*1 experiment. Contours drawn at ±0.5, 1, 2, and 3 K, with dashed contours for negative values.

[27] Figure 5a shows the equatorial stratospheric temperature anomalies resulting from the QBO-induced meridional circulation in the *Q*1 simulation. (The anomalies in temperature and circulation are determined by subtracting the 20 year mean annual cycle from the corresponding model time series). Alternating warm and cold temperature anomalies in Figure 5a descend from 35 km down to 18 km, tracking the location of the westerly/easterly shear zones, respectively, in model zonal wind (see Figure 4). The latitude–time section of model temperatures at 26 km in Figure 5b shows alternating warm and cold temperature anomalies centered on the equator and anomalies of opposite sign in the subtropics between 20° and 30° latitude. A closer examination of the equatorial temperature QBO at this level shows that the cold anomalies tend to be slightly larger (−2.75 to −3.0 K) than the warm anomalies (+2.5 K). At 20°N, the amplitude of the model temperature variations is 1 K; at 20°S, it is 1.5 K. The extratropical temperature response is strongest in both hemispheres during the late winter/early spring months. These features are consistent with the observed hemispheric asymmetry and seasonal synchronization of the extratropical QBO in lower stratospheric temperature due to horizontal momentum advection by the meridional circulation [*Jones et al.*, 1998].

[28] The modeled QBO in residual vertical velocity $\bar{w}^*$ at 26 km from experiment *Q*1 is shown in Figure 6. We find that the temperature and vertical velocity anomalies at this level are of opposite phase, with the peak temperature response leading the zonal wind by approximately 6 months, in agreement with the QBO circulation derived from meteorological analyses [*Randel et al.*, 1999]. Although the amplitude of the model temperature QBO in Figure 5 agrees with observations, the amplitude of the QBO in model $\bar{w}^*$ (±0.2 mm s^{-1} at 24 km) is almost twice as large as that reported by *Randel et al.* [1999] based on United Kingdom Meteorological Office (UKMO) meteorological analyses. Because the UKMO analyses systematically underestimate extrema in equatorial zonal wind vertical shear, and thus $\bar{w}^*$, at levels above 50 hPa [*Randel et al.*, 1999], it is likely that the amplitude of the real variation lies between the lower limit set by observations and the upper limit set by the model calculations presented here. Recent estimates of QBO variations in $\bar{w}^*$ of 0.10–0.15 mm s^{-1} between 20 and 40 hPa were reported by *Niwano and Shiotani* [2001] based on trace gas measurements from the HALOE instrument. It should be noted that their study also found a 2–3 month phase difference between interannual variations in the temperature and vertical velocity fields and a very small (<0.05 mm s^{-1}) annual variation in $\bar{w}^*$ in the region between 30 and 70 hPa.

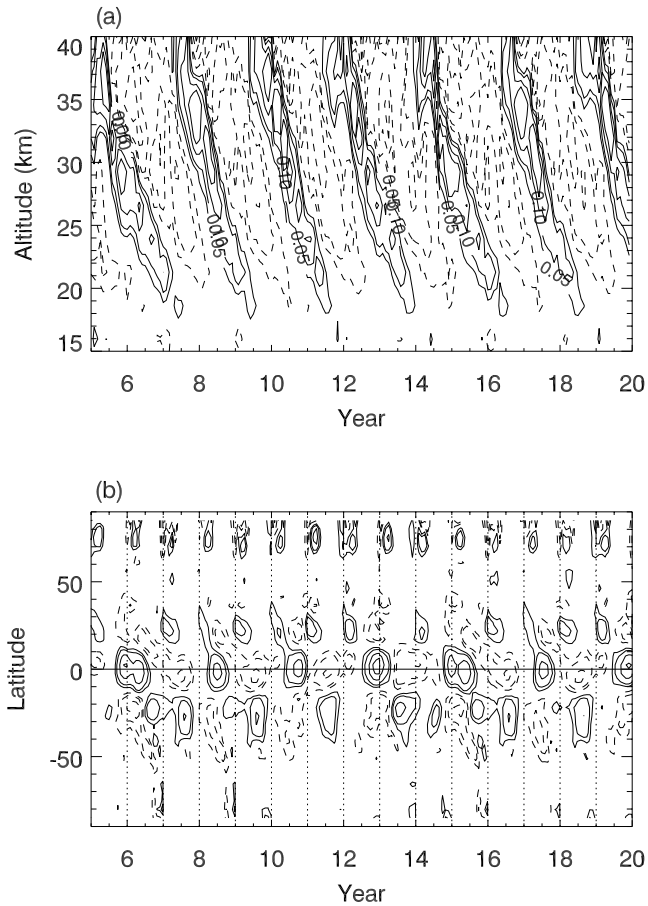

Figure 6. Same as Figure 5, but for model residual vertical velocity ($\bar{w}^*$) anomalies. Contours drawn at ±0.05, ±0.1, ±0.2, and ±0.3 mm s^{-1}.

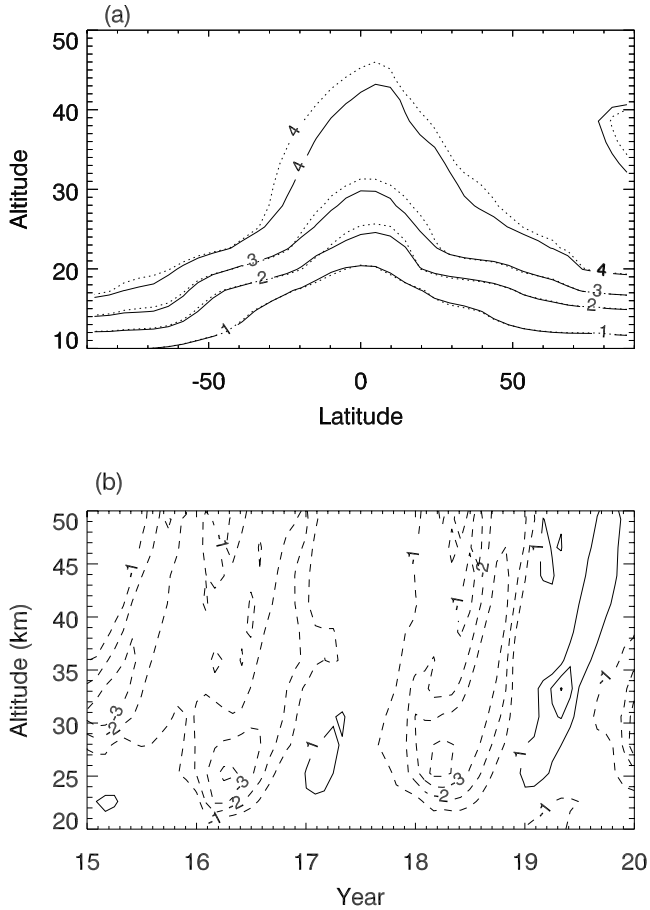

Figure 7. (a) Mean age of air (in years) from experiments $Q0$ (solid contours) and $Q1$ (dashed contours). (b) Time–altitude plot of the difference in mean age of air at the equator between experiments $Q1$ and $Q0$. Contour interval is 1 month. Dashed contours denote negative values.

This differs from the annual cycle in model vertical velocity throughout this region, which ranges in amplitude from 0.5 to 1.0 mm s^{-1}. Although detailed comparisons of recent observations and model results are beyond the scope of the present work, these apparent discrepancies need to be addressed if we are to fully understand the impact of the QBO on tracer transport. Table 2 shows that, in addition to the magnitude of QBO anomalies in $\bar{w}^*$, models must also capture the observed asymmetry in descent rates and the magnitude of the zonal wind shear.

[29] *Cordero and Nathan* [2000] noted that the larger negative QBO temperature anomalies are a consequence of the stronger easterly shear zones generated over the equator by the parameterized Rossby-gravity wave mode. This is reflected in the model residual vertical velocity ($\bar{w}^*$) anomalies plotted in Figure 6, where positive (upward) anomalies at the equator are larger than the negative (downward) anomalies. Also note the shorter duration of positive $\bar{w}^*$ anomalies compared to negative $\bar{w}^*$ anomalies in Figure 6. This is a consequence of the slower westerly descent and the longer westerly QBO phase at 26 km, on average, as compared to observations (Table 2). While lower stratospheric ascent is present throughout the entire year, the QBO will act to increase or decrease the ascent rate depending on the sign of the zonal wind shear, its strength, and duration. The overall effect of the modeled QBO is to produce stronger ascent due to the weaker westerly shear and stronger easterly shear, contrary to what is observed.

[30] This overall enhancement of upward motion throughout the equatorial lower stratosphere due to the QBO has implications for model estimates of the mean age of air, which is a useful diagnostic for model transport of stratospheric tracers [*Hall and Plumb*, 1994]. The mean age of air is determined from the transport of a fictitious tracer with a time-dependent tropospheric source and no chemical loss or horizontal eddy mixing (this is the "unmixed age" described by *Bacmeister et al.* [1998]). With this definition, any differences in the mean age of air will be due solely to differences in the vertical transport of the tracer from the source region. Figure 7a compares the mean age of air for a fictitious long-lived trace constituent in experiments $Q0$ (no QBO) and $Q1$ (with QBO). Between 5°N and 5°S latitude, the difference in the age of air produced by the QBO (Figure 7b) ranges from 3 to 4 months, and the largest differences are found between 25 and 30 km altitude. The presence of the QBO acts to reduce the modeled mean age of air in the stratosphere by increasing the overall ascent rate of air in the tropical lower stratosphere due to stronger easterly shear compared to westerly shear in the modeled zonal winds. Most two-dimensional and three-dimensional models without a QBO significantly underestimate the mean age of air as derived from constituent observations [*Hall et al.*, 1999]. Based on the results shown in Figure 7, including the QBO will improve the modeled interannual variability in transport of H_2O and CH_4, but will not significantly affect age of air calculations.

3.2. Sensitivity of the Model QBO to External Forcing

[31] Within the TEM formulation of the model, the equatorial zonal wind tendency in the lower stratosphere (i.e., below 30 km) can be expressed as

$$\frac{\partial \bar{u}}{\partial t} = -\bar{v}^*\left(\frac{\partial \bar{u}}{a\partial \phi}\right) - \bar{w}^*\frac{\partial \bar{u}}{\partial z} + \bar{X} \qquad (6)$$

where $\bar{X}$ represents the QBO forcing (equation (3)) and we have neglected the extratropical planetary wave, gravity wave, and Coriolis terms. Model calculations show that the vertical momentum advection term in equation (6) is much larger than the horizontal momentum advection term. This implies that the modeled QBO in zonal winds can be influenced by both the specified tropical momentum source $\bar{X}$ and by the strength of the vertical component of the residual circulation ($\bar{w}^*$) in the equatorial lower stratosphere. In this section, we examine the sensitivity of the modeled zonal wind QBO simulation to changes in the strength of the dynamical and thermal forcing of the meridional circulation.

[32] *Bacmeister et al.* [1998] found that both $\bar{w}^*$ and the mean age of air in CHEM2D simulations are sensitive to changes in the prescribed model latent heating profiles in the tropical troposphere. These earlier simulations were performed without coupling between the model dynamics and photochemistry, and net radiative heating rates were computed from climatological distributions of ozone,

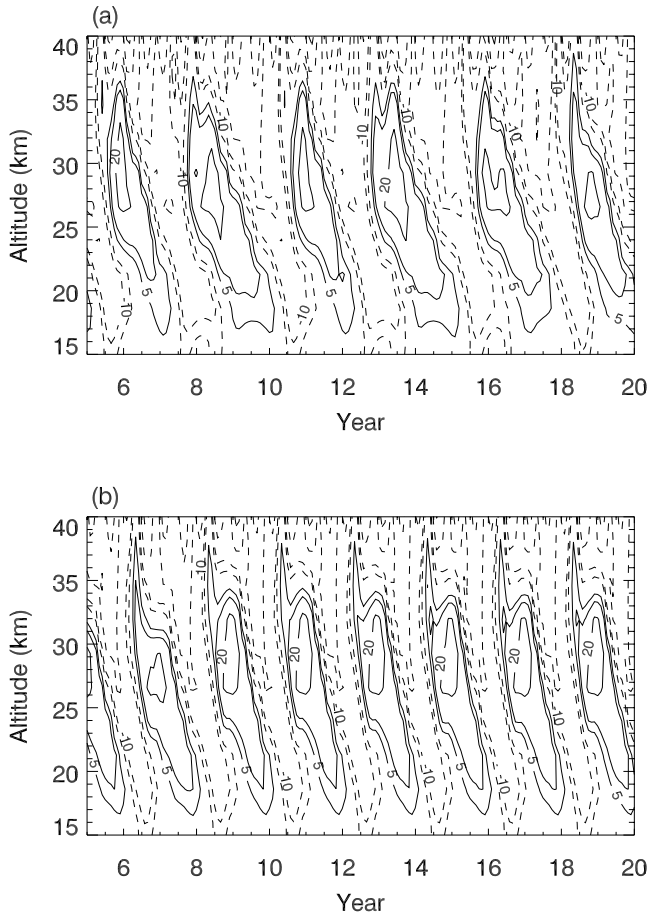

Figure 8. Equatorial zonal wind profile from the *Q*4 (a) and the *Q*5 (b) experiments in which the NH planetary wave forcing is decreased and increased by 25%, respectively. Contours drawn at ±5, ±10, ±20, and ±30 m s^{-1}.

water vapor, etc. To determine the effect of these heating changes on the modeled QBO in the coupled model, two simulations were performed in which the prescribed latent heating $\mathcal{H}_{LH}$ was decreased or increased everywhere by 25% (experiments *Q*2 and *Q*3, respectively). When compared to the baseline QBO simulation *Q*1, the time mean vertical profiles of $\bar{w}^*$ averaged between 10°N and 10°S latitude from the *Q*2 and *Q*3 runs show a weak dependence on the strength of the prescribed latent heating, with larger heating producing slightly increased ascent. Increasing the latent heating by 25% lengthens the period of the QBO in the *Q*3 run by 1 month compared to the *Q*1 simulation. A 25% decrease in the latent heating does not change the QBO period at all. Thus the effect of these heating changes on the period of the zonal wind QBO is marginal.

[33] As noted in section 1, ascent in the tropical stratosphere is also controlled by extratropical planetary wave forcing in the winter hemisphere. *Dunkerton* [1991] demonstrated that an increase in the imposed extratropical forcing produces stronger ascent and a longer QBO period in an idealized two-dimensional model, while a decrease in the imposed forcing produces the opposite effect. The modeling study of *Kinnersley and Pawson* [1996] showed that an increase in diabatic heating in the equatorial lower stratosphere should lead to a stalling of the zero wind line, particularly in the easterly phase of the QBO, which also increases the QBO period. In their model, changes in lower stratospheric heating rates were introduced when the effect of planetary wave activity on tropical ozone was included. In the present study, two additional simulations were carried out to determine how the modeled QBO period responds to changes in the strength of the planetary wave forcing through the EP flux divergence term in equation (1). In these simulations, the amplitude Z_{NH} of the Northern Hemisphere planetary wave forcing at the model lower boundary was decreased (experiment *Q*4) and increased (experiment *Q*5) by 25% relative to the *Q*1 simulation (see Table 1).

[34] In Figure 8a, the descent of the easterly QBO phase is delayed in the *Q*4 case, and the period of the QBO is extended to 30 months. In the *Q*5 case (Figure 8b), the more rapid descent of the QBO easterlies produces a 24 month QBO. This result may seem to contradict earlier studies that show an increase in the QBO period as extratropical planetary wave drag increases [e.g., *Dunkerton*, 1991]. Why then does the larger imposed planetary wave amplitude in experiment *Q*5 produce a shorter QBO period? As shown in Figure 9a, a larger planetary wave

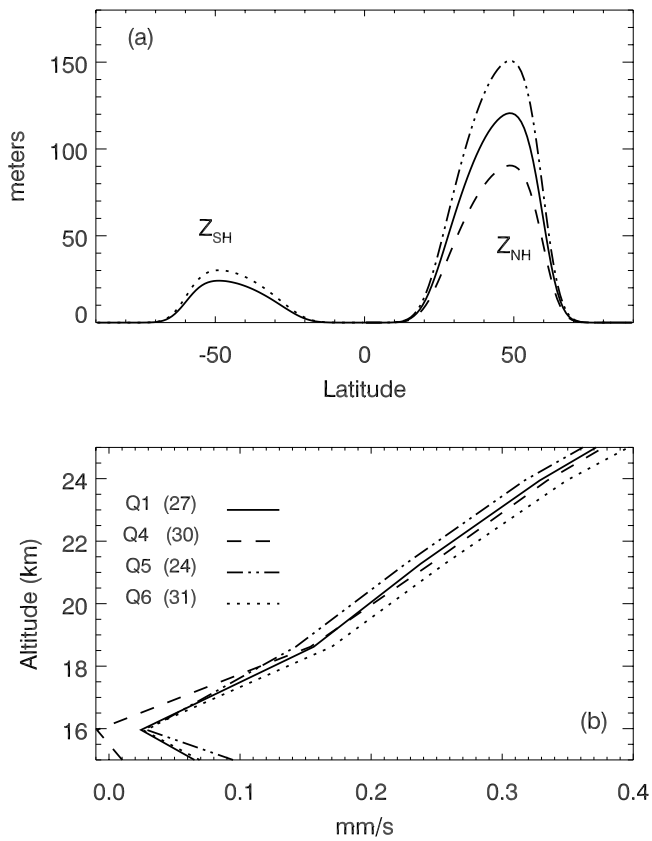

Figure 9. (a) Meridional profile of the planetary wave amplitudes at the model lower boundary for the *Q*1 (solid line), *Q*4 (dashed), *Q*5 (dot-dashed), and *Q*6 (dotted) experiments. (b) Vertical profiles of annual mean $\bar{w}^*$ at the equator for the four experiments in (a). The period of the equatorial zonal wind QBO (in months) at 26 km for each experiment is shown in parentheses.

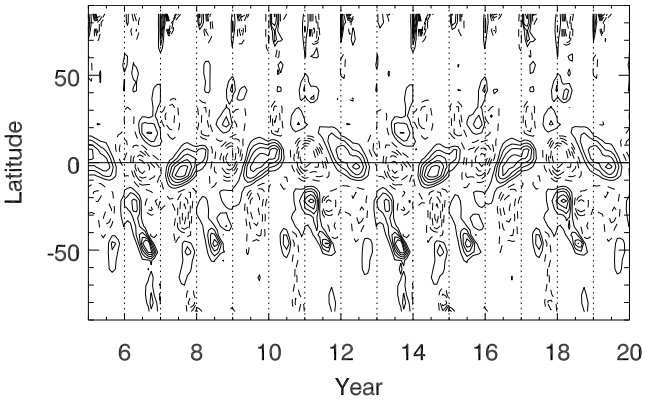

Figure 10. Latitude–time section of zonal mean temperature at 26 km from experiment *Q*3 with increased latent heating. Contours drawn every 0.5 K. Dashed contours denote negative values.

amplitude is adopted in the NH to produce a realistic hemispheric asymmetry in the wintertime zonal wind fields (Figure 1). The larger amplitude wave is closer to "saturation," and so increasing its amplitude further will primarily affect the location of maximum EP flux divergence rather than changing its overall strength [*Bacmeister et al.*, 1998, Figure 8]. When the wave forcing is increased in the *Q*5 experiment, there is an increase in EP flux divergence in the Northern midlatitudes below 20 km, and a decrease in EP flux divergence above 20 km. The annual average $\bar{w}^*$ at the equator in the *Q*5 experiment, plotted in Figure 9b, responds accordingly, increasing below 20 km and decreasing above 20 km. Reducing the NH wave amplitude has the opposite effect on the vertical velocity profile and the period of the QBO.

[35] To further illustrate this point, an additional model run (*Q*6) was performed in which the planetary wave amplitude Z_{SH} was increased by 25%. The result is an increase in $\bar{w}^*$ throughout the stratosphere and a QBO period of 31 months (Figure 9b). Because the SH wave amplitude is much smaller than its NH counterpart, it is farther from becoming saturated and so the large-scale circulation response conforms to previous expectations, i.e., increased wave amplitude produces greater extratropical forcing and stronger equatorial upwelling. From these results we conclude that the sensitivity of the QBO to changes in extratropical forcing is dependent not only on the magnitude of these changes but also on their location, a conclusion in accord with the sensitivity studies performed by *Plumb and Eluszkiewicz* [1999] with their nonlinear two-dimensional model.

3.3. Low-Frequency Variability

[36] The preceding series of model experiments demonstrates that the period of the QBO is less sensitive to changes in latent heating than to changes in the strength of the extratropical planetary wave activity that drives the meridional circulation. Although the uniform ±25% differences in mechanical and thermal forcing used in our sensitivity experiments may be unrealistic, it is conceivable that comparable variations in the latent heating or planetary wave amplitudes over localized regions more typical of natural interannual variability could introduce changes in the period of the QBO of a few months. Such changes could produce a range of low-frequency oscillations in lower stratospheric temperatures and ozone that arises from the phasing of the QBO-induced meridional circulation and the seasonal cycle [*Gray and Dunkerton*, 1990].

[37] For example, the QBO signal in extratropical temperatures at 26 km from the *Q*1 model simulation (Figure 5, bottom panel) exhibits a modulation in both hemispheres with a period of ~9 years. Spectral analysis of the model zonal wind time series at 26 km [*Ghil et al.*, 2002] shows a peak at 27 months, meaning the maximum easterly/westerly phase of the QBO will coincide with the stronger winter hemisphere circulation once every 4 cycles, which results in a beat period of 9 years. This is seen in temperature anomalies at 26 km between 20° and 40° latitude from the *Q*1 experiment shown in Figure 5. This low-frequency variability is also seen in model ozone and water vapor throughout the lower stratosphere (not shown).

[38] Figure 10 shows that changes in the QBO period will result in different beat periods in the extratropical QBO signal. In the *Q*3 experiment, the resulting 28 month QBO now produces a beat period of 7 years in the extratropical temperature response at 26 km. The *Q*5 experiment produces a QBO period of 2 years, in which case the QBO and seasonal cycle are always in phase and there is no low-frequency signal present in the extratropics. The relationship between the period of the QBO and the low-frequency variability in the extratropical signal (Figure 11) is such that variations of 5–15 years are possible for the typical range of QBO periods that is observed. Because the interaction between the QBO and the wintertime meridional circulation impacts the zonally averaged transport of trace constituents in the subtropics, the period of the QBO can influence the decadal variability in species such as ozone and water vapor. Similarly, the QBO period may also modulate decadal-scale variability at high latitudes in the upper stratosphere and

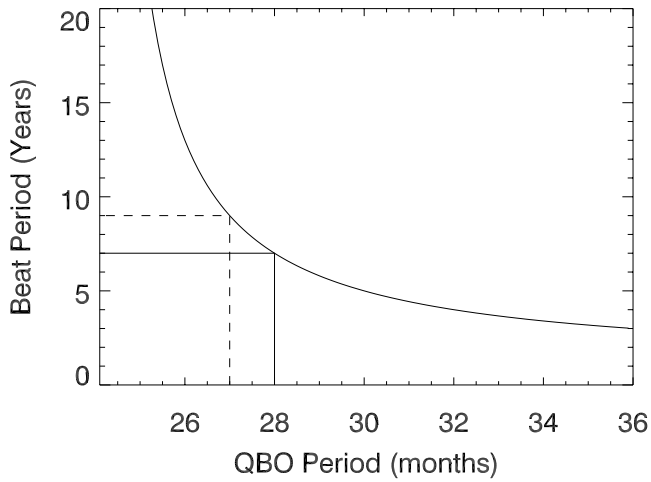

Figure 11. The beat period (in years) produced by the phasing of the equatorial QBO and the seasonal cycle as a function of QBO period (in months).

Table 3. Dependence of Water Vapor QBO on Model Lower Boundary Condition

		Amplitude of QBO in H_2O (ppmv)				
Experiment	Boundary condition	15 km	20 km	25 km	30 km	35 km
*Q*1	fixed annual cycle	0.005	0.062	0.104	0.120	0.128
*W*2	no annual cycle (constant)	0.000	0.015	0.047	0.097	0.131
*W*3	interactive annual cycle	0.229	0.129	0.126	0.148	0.125

mesosphere through the filtering of gravity waves by successive easterly and westerly QBO regimes [*Mayr et al.*, 2000].

4. The QBO in H_2O and CH_4

[39] This section describes simulations of the QBO in stratospheric H_2O and CH_4 produced by the three experiments listed in Table 3. Each experiment uses a different lower boundary condition for the water vapor mixing ratio at the tropical tropopause. The *Q*1 simulation (same as listed in Table 1) has an imposed sinusoidal variation in H_2O mixing ratio at 15 km in the tropics with an amplitude of 1 ppmv and a period of 1 year whose phase is adjusted to match the observed annual cycle (see Figure 2a, solid curve). This so-called fixed lower boundary condition on the equatorial H_2O mixing ratio makes it possible to isolate the part of the modeled H_2O QBO that is due solely to transport, i.e., it does not include the QBO in tropical tropopause temperatures modifying the entry value of H_2O into the lowermost stratosphere. The *W*2 model run has a constant water vapor lower boundary condition (i.e., no "tape recorder"), in which the mixing ratios are kept at 3.5 ppmv throughout the entire troposphere. Comparing the results of experiments *W*2 and *Q*1 illustrates the dependence of the lower stratospheric H_2O QBO on the presence of an imposed annual cycle in water vapor at the tropical tropopause [see also *Geller et al.*, 2002]. The *W*3 experiment uses a fully interactive lower boundary condition in which the mixing ratios at the tropical tropopause vary according to the model temperatures in that region (see Figure 2a, dashed curve). Since these temperatures include a QBO signal, the resulting H_2O anomalies in experiment *W*3 represents the combined effects of the QBO in transport and in the temperature variability of the tropical tropopause region.

[40] Figure 12a shows the model equatorial H_2O anomalies from year 5 to year 20 in model run *Q*1. Alternating positive and negative anomalies of 0.05–0.1 ppmv are present between 20 and 40 km (see Table 3). The anomalies between 28 and 35 km are opposite in sign from the lower stratospheric anomalies. At 30 km (Figure 12b), the largest H_2O anomalies are found in the subtropics during the winter months. Figure 13 depicts the structure of the $\bar{v}^*$ anomalies superimposed upon the background H_2O mixing ratio distribution. During periods of westerly shear (Figure 13a), the QBO-induced circulation anomaly consists of a downward perturbation in vertical velocity over the equator between 20 and 30 km, which produces convergent $\bar{v}^*$ anomalies near 30 km and a divergent $\bar{v}^*$ near 20 km. These convergent anomalies in $\bar{v}^*$ advect air with higher moisture content from the subtropics, producing a positive equatorial water vapor anomaly at 30 km. During periods of easterly shear (Figure 13b), the situation is reversed, with a positive $\bar{w}^*$ anomaly over the equator producing divergent $\bar{v}^*$ anomalies and a negative water vapor anomaly near 30 km.

[41] The occurrence of large H_2O anomalies in the subtropics at 30 km during late winter and early spring (Figure 12b) months suggests that these anomalies originate from advection by the QBO-induced meridional circulation [e.g., *Jones et al.*, 1998]. This can be seen by examining the interannual variability in each of the terms on the right hand side of the tracer tendency equation (equation (5)). The largest contributions to the interannual variability in the H_2O tendency equation at 30 km and 20°N come from vertical advection, meridional advection, and horizontal eddy diffusion. Net photochemical sources are not negligible in the tendency equation, but their interannual variability is small; the vertical diffusion term is much smaller than any of the other terms and can be neglected.

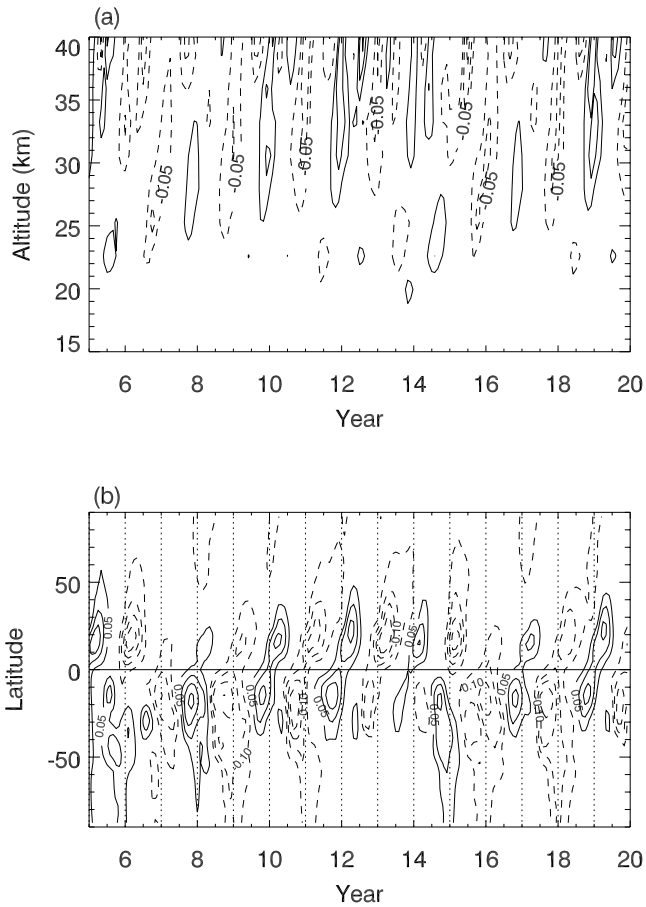

Figure 12. (a) Model QBO anomalies (climatological annual cycle removed) in equatorial water vapor and (b) water vapor anomalies at 30 km from the *Q*1 experiment. Contour interval is 0.05 ppmv. Dashed contours indicate negative values.

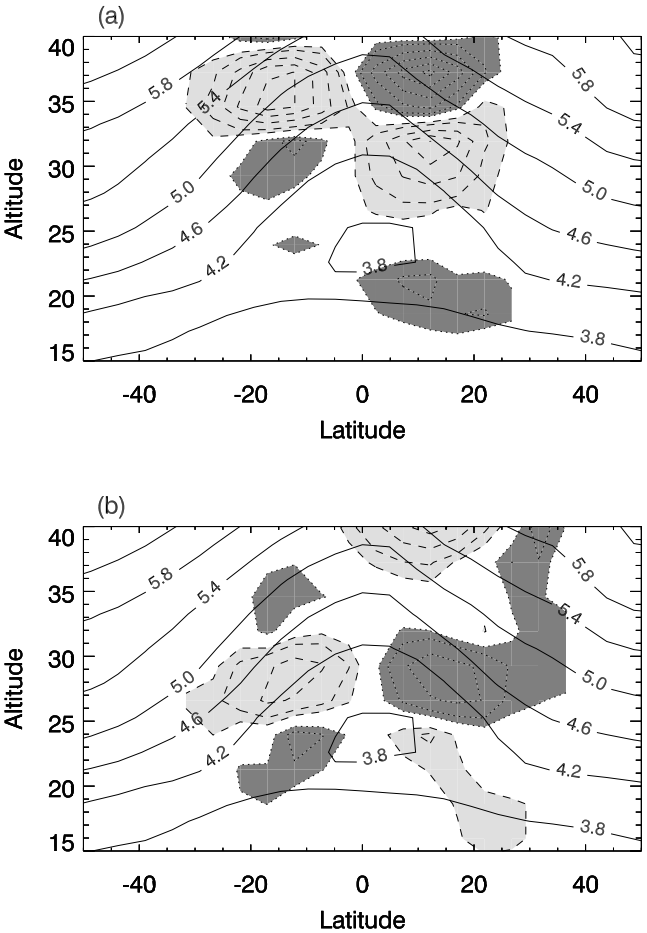

Figure 13. (a) Anomalies in meridional velocity $\bar{v}^*$ (dashed contours for negative, dotted contours for positive) on day 91, year 12 of experiment $Q1$ during the descending westerly phase of the QBO, superimposed upon the background water vapor mixing ratio from experiment $Q0$ (solid contours). (b) Same as in (a), but for day 331, year 12 of experiment $Q1$ during the descending easterly phase of the QBO.

[42] As the results from the $Q1$ experiment in Figure 14a show, there is considerable variability in the meridional advection component associated with the QBO consisting of stronger negative tendencies during the easterly phase (e.g., years 11 and 13) and weaker negative tendencies during the westerly phase (e.g., years 10, 12, and 14). The contribution of this term to the net H_2O tendency is seen by comparing the sum of the three terms (meridional advection, vertical advection, and horizontal eddy diffusion) from the $Q1$ experiment in Figure 14b (black curve) with the $Q0$ experiment (gray curve). As compared to the baseline $Q0$ case (no QBO), the more negative net tendencies leading up to winter/spring in years 11 and 13 in the $Q1$ run from the meridional advection term will promote lower H_2O mixing ratios overall. The opposite is true in the months leading up to winter/spring of years 12 and 14, where the less negative meridional advection term promotes higher H_2O mixing ratios as compared to the $Q0$ case. Analysis of the CH_4 tendency terms (not shown) yields similar results although of opposite sign. While model values of the horizontal eddy diffusion K_{yy} in this region have larger values during the westerly QBO phase and smaller values during the easterly phase, the meridional gradient in K_{yy} is not greatly affected and so horizontal eddy diffusion produces a smaller contribution to the interannual variability in the tracer tendencies. The primary role of meridional transport in producing tracer anomalies supports the conclusions drawn from recent observational analyses of O_3, CH_4, and H_2O [*Gray and Russell*, 1999; *Dunkerton*, 2001].

[43] Since the distributions of H_2O and CH_4 in the middle atmosphere are closely coupled through the oxidation of CH_4 via OH, vertical and meridional gradients in middle atmospheric H_2O and CH_4 are of opposite sign. Similarly, variations in H_2O and CH_4 due to the QBO-induced circulation will also be opposite in sign. Figure 15a shows QBO anomalies in equatorial CH_4 from experiment $Q1$ with values ranging between ±0.025 and ±0.05 ppmv. The sign of the CH_4 anomalies are negatively correlated with the modeled H_2O anomalies (Figure 12). The QBO in CH_4 over the equator is only present above 28 km. Figure 15b shows the largest CH_4 anomalies at 30 km are found in the subtropics, in good agreement with HALOE observations [*Randel et al.*, 1998; *Dunkerton*, 2001]. As in the case for H_2O, analysis of the CH_4 tendencies indicates that advec-

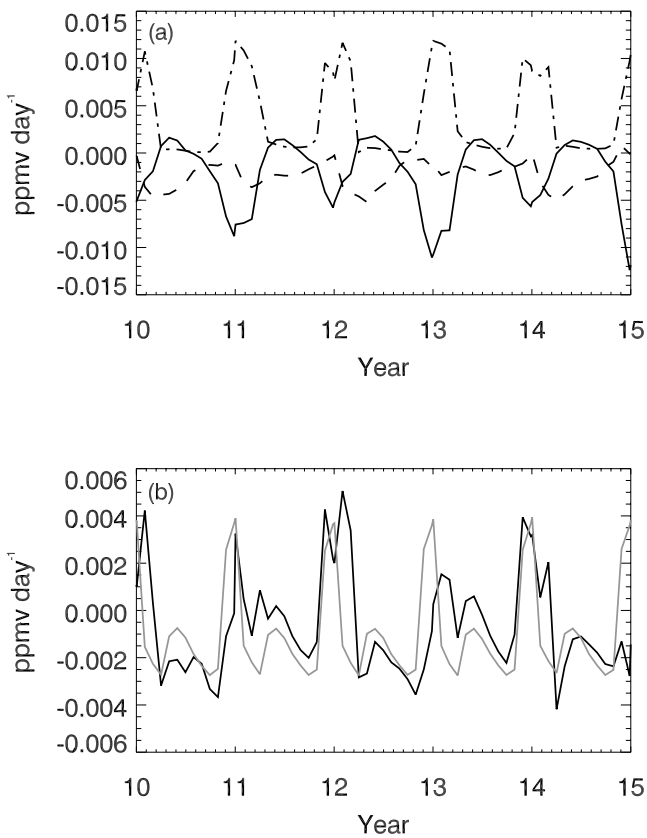

Figure 14. Components of the H_2O mixing ratio tendency equation at 30 km and 20°N from experiment $Q1$ corresponding to meridional advection (solid curve), vertical advection (dashed), and meridional eddy mixing term (dot-dashed). (b) The black curve represents the sum of all three components in (a). The gray curve is the corresponding sum from the $Q0$ experiment with no QBO.

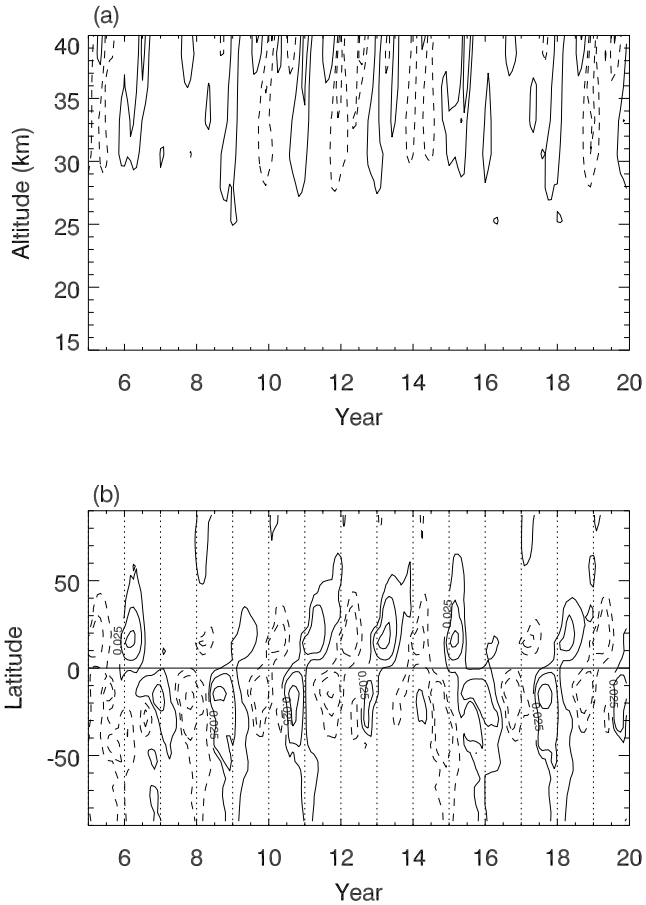

Figure 15. (a) Model QBO anomalies in equatorial CH_4 and (b) CH_4 anomalies at 30 km from the *Q*1 experiment. Contours drawn at ±0.025, ±0.05, ±0.10, and ±0.15 ppmv, with dashed contours indicating negative values.

tion by the meridional component of the residual circulation is the primary source of these anomalies.

[44] Figure 16 illustrates why a QBO in lower stratospheric H_2O mixing ratios, but not in CH_4, is due to the presence of the annual cycle in H_2O mixing ratios at the tropical tropopause. Comparing the water vapor distributions on day 91, year 12 in experiments *Q*1 ("fixed" tape recorder), *W*2 (no tape recorder), and *W*3 (tape recorder plus QBO effect) with the CH_4 distribution from the *Q*1 run, one can see that vertical and horizontal gradients in H_2O mixing ratio throughout the equatorial lower stratosphere are much more pronounced than gradients in CH_4 mixing ratio when the tape recorder effect is included (e.g., runs *Q*1 and *W*3).

[45] The role of the tape recorder effect in producing the equatorial QBO anomalies is illustrated further in Figure 17. In the absence of appreciable vertical and meridional gradients, the QBO circulation anomalies in experiment *W*2 produce little to no interannual variation in H_2O below 28 km (Figure 17a). However, when the ~0.5 K QBO in model equatorial tropopause temperatures is included in the water vapor boundary condition (experiment *W*3), the amplitude of the equatorial QBO in lower stratospheric H_2O is enhanced significantly compared to experiment *Q*1 with no QBO effect in tropopause temperatures. A comparison of the lower stratospheric water vapor anomalies in Figures 17b and 12a shows that this enhancement can be as much as a factor of two (see also Table 3). Taking the difference between the equatorial H_2O anomalies in experiments *W*3 and *W*2 (Figure 17c) reveals that the effects of the imposed lower boundary condition can extend up to 40 km.

[46] The vertical and horizontal advection terms in the equatorial H_2O and CH_4 tendencies at 21 km are shown in Figures 18 and 19, respectively, for the *Q*1, *W*2, and *W*3 experiments. In contrast to the subtropics (Figure 14), comparing Figures 18 and 19 shows that the contribution to the QBO in H_2O from vertical advection is much larger than the contribution from meridional advection. Regarding the presence of the tape recorder effect, interannual variations in the vertical advection of H_2O in the *Q*1 and *W*3 cases are much larger than in the *W*2 case (Figure 18a). In all three cases, there are vanishingly small variations in the CH_4 tendency (Figure 18b). Similarly, the QBO in meridional advection of H_2O in the *Q*1 case is much larger than in the *W*2 case, and larger still in the *W*3 case (Figure 19a), but no similar dependence is found in the CH_4 tendency (Figure 19b). One caveat regarding the enhancements in the modeled water vapor QBO seen in experiment *W*3 is that the model may overestimate such an effect by assuming that the QBO in zonally averaged equatorial temperature controls the H_2O mixing ratio lower boundary condition over the entire model domain. In the real atmosphere, sources of lower stratospheric H_2O from tropical convection have a pronounced zonal dependence [*Jackson et al.*, 1998], and it is not entirely clear how the lower stratospheric temperature QBO affects these sources.

5. Summary and Discussion

[47] An interactive parameterization for the QBO has been implemented in a zonally averaged photochemical–dynamical model to investigate the effect that interannual variations in the mean meridional circulation of the equatorial stratosphere have on the distribution of H_2O, CH_4, and mean age of air in the stratosphere. One advantage of this approach is that the period of the QBO is not imposed, but free to vary according to the mechanical and thermodynamic forcing of the model circulation. We find that the period of the QBO is more sensitive to changes in the specified planetary wave forcing and less sensitive to changes in the prescribed latent heating attributed to convective activity near the tropopause. However, the response of the mean meridional circulation to changes in planetary wave forcing, and its effect on the period of the QBO, depends on whether they are imposed in the Northern or Southern Hemisphere.

[48] In the Southern Hemisphere, a 25% increase in planetary wave amplitude leads to stronger tropical upwelling and a longer QBO period (31 months compared with 27 months in the baseline experiment). The same increase in Northern Hemisphere planetary wave amplitude leads to weaker tropical upwelling above 20 km, thereby reducing the QBO period by 3 months, contrary to what one might expect. The difference in the response of the QBO between the *Q*5 and *Q*6 experiments is explained by the differences in the imposed planetary wave forcing in each hemisphere. The larger planetary

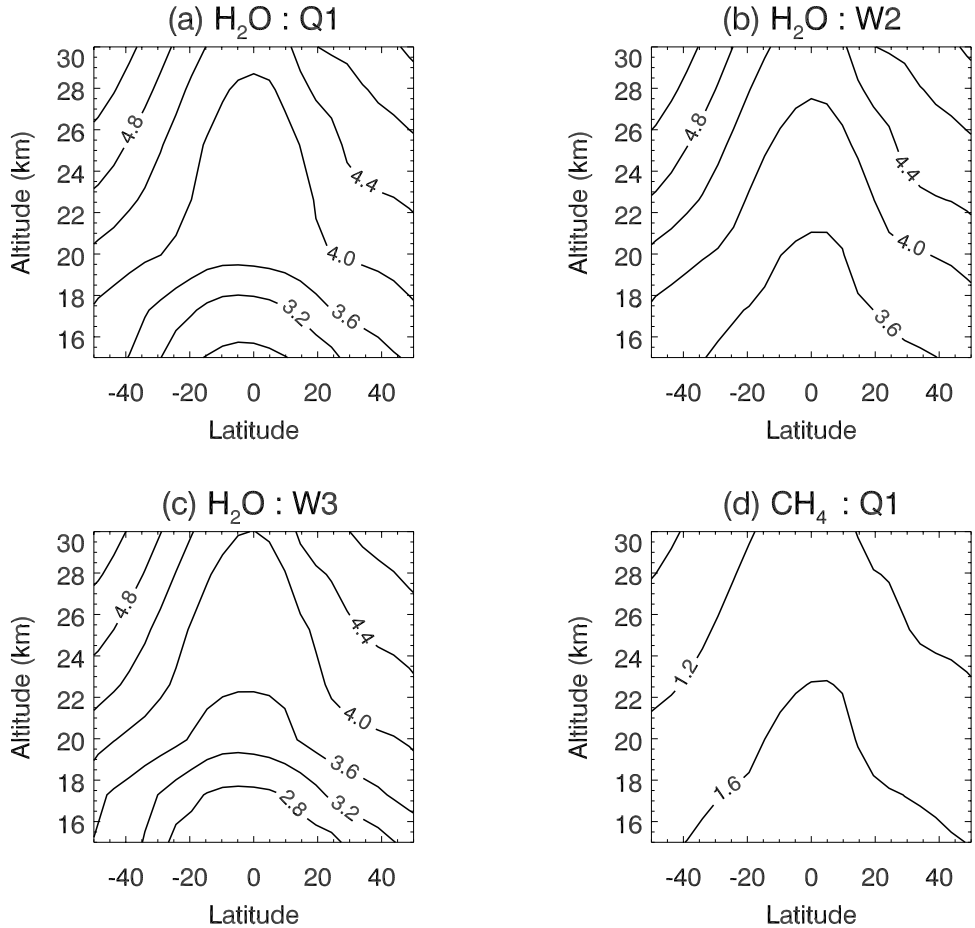

Figure 16. Latitude–altitude plots of H_2O mixing ratio on day 91, year 12 of experiment *Q*1 (a), *W*2 (b), and *W*3 (c). Corresponding latitude–altitude plot of CH_4 mixing ratio in experiment *Q*1 (d). Contours are drawn every 0.4 ppmv.

wave amplitudes in NH are much closer to saturation, so further increases result in additional drag lower down and reduced drag higher up. Decreasing the wave forcing in the NH has the opposite effect. The smaller wave forcing in the SH means that the waves are much farther from saturation, and so an increase in the forcing at the lower boundary produces increased drag throughout the extratropical winter stratosphere. The responses of both tropical upwelling in the stratosphere and the QBO period to changes in the strength of planetary wave forcing in the NH can be classified as nonlinear, while the responses to changes in the SH forcing can be classified as linear. The variable length of the QBO period is important, since the phasing of the QBO with the annual cycle can produce low-frequency (i.e., decadal) modulation of the QBO signal in constituent fields within and without the tropical stratosphere. Our results show that the origins of quasi-periodicity in the QBO may arise as a complex response to changes in the strength of both tropical and extratropical forcing mechanisms.

[49] An annually varying lower boundary condition in modeled H_2O mixing ratio at the tropical tropopause has also been included to simulate the observed atmospheric "tape recorder" effect. This allows the moisture content of air parcels entering the lower stratosphere to vary according to the modeled annual cycle in tropical tropopause temperature. Without this feature, the modeled QBO in equatorial water vapor is confined to altitudes of 30–40 km. With this feature, the model produces a QBO anomaly of 0.1 ppmv in the region between 25 and 30 km. This is comparable to the observed interannual anomalies of 0.1–0.2 ppmv in HALOE H_2O reported by *Randel et al.* [1998]. When the effect of the QBO is included in the model tropopause temperatures, the H_2O QBO between 15 and 20 km is significantly larger. The presence of a QBO in H_2O mixing ratio but not in CH_4 below 30 km can be explained by the interaction between the modeled annual cycle in lower stratospheric H_2O and the QBO-induced meridional circulation anomalies. The model calculations show that the tropical H_2O anomalies at and below 30 km are produced mainly through transport by the QBO-induced meridional circulation, while QBO modulation of eddy transport plays a smaller role.

[50] The strength of the QBO-induced meridional circulation anomalies are coupled with the seasonal cycle, i.e., they are strongest in the winter hemisphere [*Jones et al.*, 1998]. This coupling produces a hemispheric asymmetry in

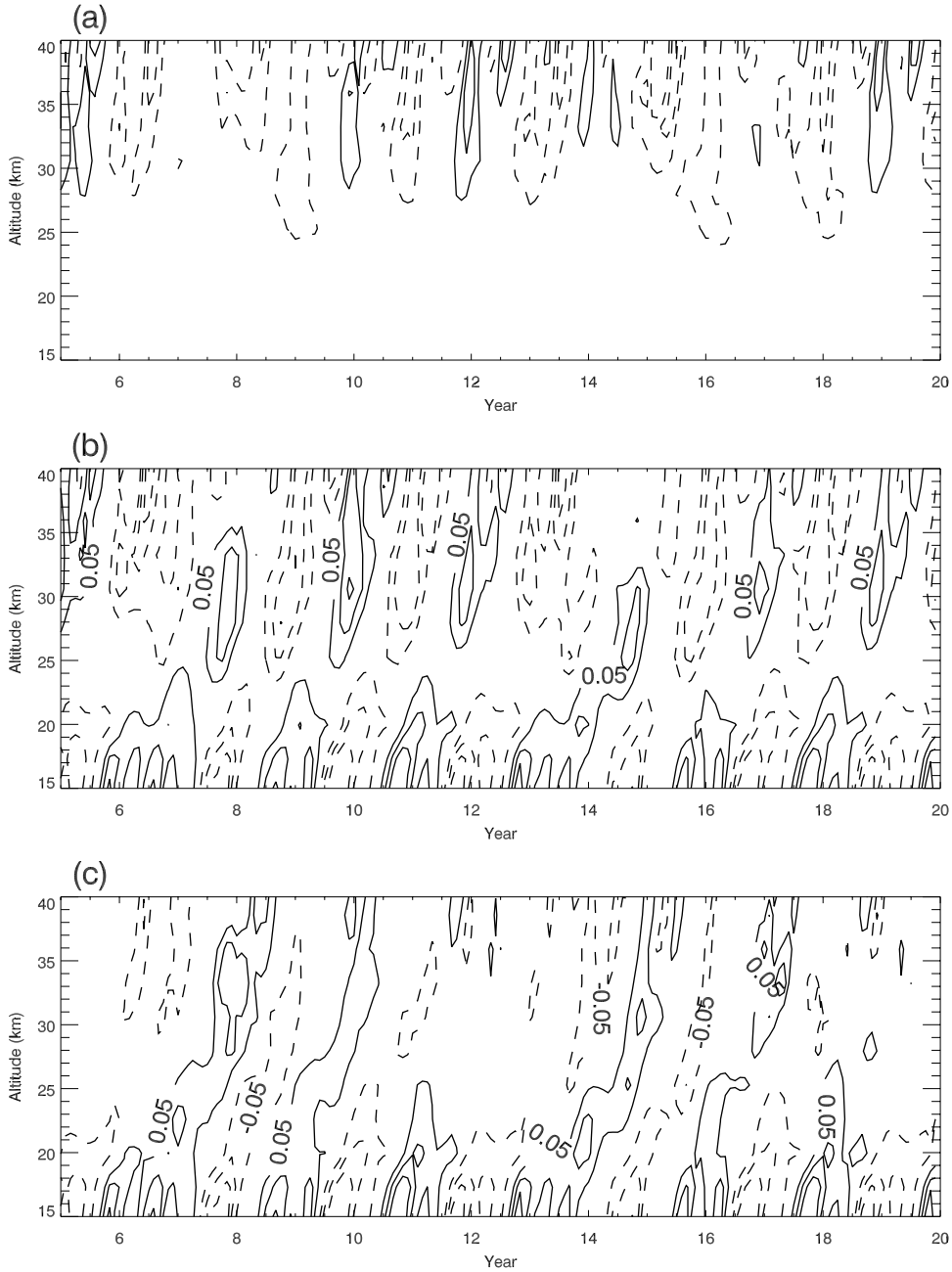

Figure 17. Altitude–time plot of QBO anomalies in equatorial H_2O mixing ratio from model simulations (a) *W*2 and (b) *W*3 and their difference (c). Contours are drawn every ±0.05, 0.1, 0.2, and 0.3 ppmv, with dashed lines for negative values.

the constituent QBO anomalies having a maximum at subtropical latitudes. The 20 year simulations show that this coupling produces a low-frequency beating in the subtropical QBO signal, and this frequency depends on the QBO period. The 27 month QBO period in the coupled simulation produces a 9 year modulation that is seen in model temperature, H_2O, and CH_4 anomalies. However, this low-frequency variation results from an unrealistic condition, i.e., that the period of the QBO does not change throughout the course of the simulation. In the real atmosphere, the period of the QBO can be as short as 24 months and as long as 34 months. It is desirable, therefore, to determine what processes lead to this quasi-periodic behavior and how they might be incorporated into the existing model. Based upon our initial findings concerning the roles of both planetary wave activity and tropical latent heating in determining the model QBO period, it is possible that including realistic variations in these quantities on seasonal and interannual timescales could provide the necessary quasi-periodicity within the existing two-dimensional model framework.

[51] Although the present model formulation successfully reproduces many of the observed features of the QBO in H_2O and CH_4 at 30 km and below, the simulation

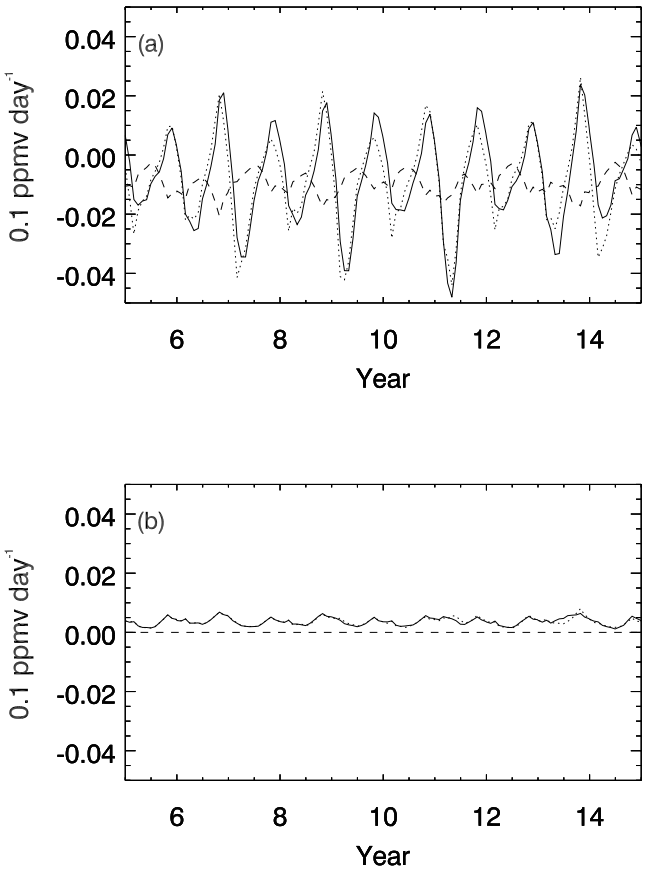

Figure 18. Time series of the vertical advection term in the mixing ratio tendency equation at 21 km from experiments *Q*1 (solid curve), *W*2 (dashed), and *W*3 (dotted) for equatorial H_2O (a) and CH_4 (b).

does not adequately capture the interannual variability above 40 km. In their analysis of HALOE measurements, *Randel et al.* [1998] report that the QBO in equatorial CH_4 maximizes near 40 km, and is accompanied by a QBO in H_2O at 40 km that is opposite in phase from the water vapor QBO near 30 km. This observed behavior is a consequence of strong vertical velocity anomalies over the equator at 40 km deduced from meteorological analyses [*Randel et al.*, 1999]. The modeled QBO in equatorial vertical velocity peaks well below 40 km, and therefore does not generate the large variations in water vapor and methane that are observed. This may be due to deficiencies in the parameterization of the QBO, or it may be due to the lack of a realistic SAO in equatorial zonal winds near the stratopause. In the model, easterly flow persists during the entire year over the equator between 40 and 55 km. Rocketsonde data show alternating easterly and westerly flow in this region, with the occurrence of the westerlies 2–3 months after the solstices [*Garcia et al.*, 1997]. The unrealistic upper stratospheric equatorial winds in the model may prevent alternating easterly and westerly shear zones from forming due to QBO forcing, thereby limiting the temperature and vertical velocity anomalies at and above 40 km. Previous observational and diagnostic modeling studies of subtropical tracer transport by the QBO [*Gray and Russell*, 1999; *Gray*, 2000] have suggested that the relative roles of advection and eddy transport are altitude dependent, with eddy transport becoming more important in the middle and upper stratosphere. This highlights the need for an accurate simulation of an interactive SAO in the equatorial upper stratosphere in order to properly describe interannual variations in tracer transport throughout the stratosphere.

[52] These interactive model simulations have shown that the QBO has a substantial impact on the interannual variability in stratospheric H_2O and CH_4 that extends to decadal timescales. These simulations have also shown that the QBO itself is sensitive to the strength of the mechanisms that drive the residual meridional circulation. In the case of H_2O, the QBO causes variations directly through advection by mean meridional circulation anomalies, and indirectly through modulation of tropical tropopause temperatures. This source of natural variability should be accounted for when considering long-term changes in stratospheric composition. For example, a recent study by *Waugh et al.* [2001] finds the total chlorine abundance in the upper stratosphere is decreasing faster than expected since 1997. This behavior may be due to decadal variability in the transport of constituents such as H_2O and CH_4 that control the catalytic destruction of ozone in this region. Model simulations with a realistic QBO that is sensitive to changes in dynamical and thermal forcing of the meridional circulation can improve our understanding of observed long-term changes in radia-

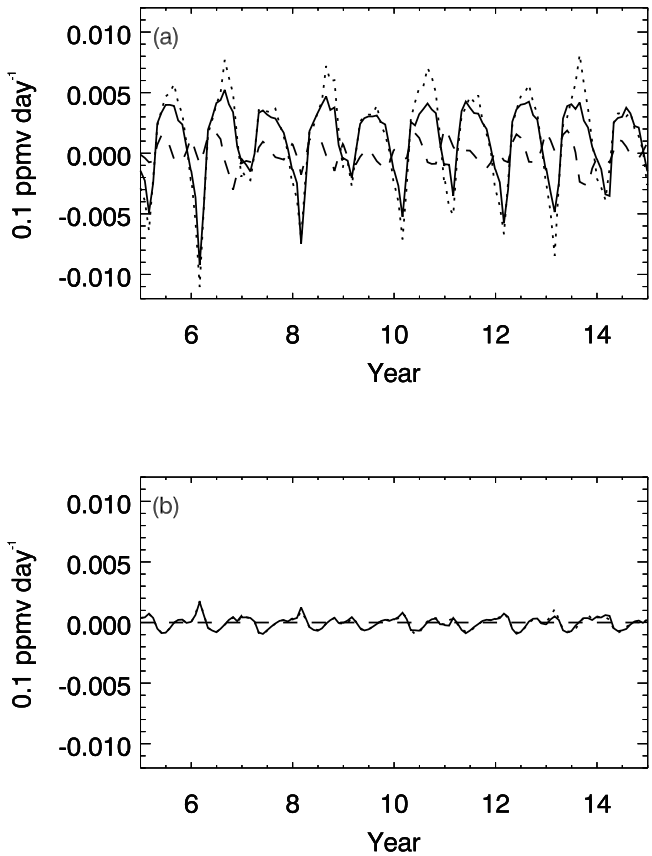

Figure 19. Same as in Figure 18, but for the meridional advection term.

tively active constituents such as water vapor and ozone, and thereby aid in future assessments of the middle atmospheric response to these changes.

[53] **Acknowledgments.** Support for this work at NRL has come from the Office of Naval Research. The updated Singapore wind data provided by Barbara Naujokat was obtained through the UCAR Data Support Section. The authors gratefully acknowledge helpful comments by S. D. Eckermann and two anonymous reviewers that led to substantial improvements of this manuscript.

References

Andrews, D. G., J. R. Holton, and C. B. Leovy, *Middle Atmosphere Dynamics*, 489 pp., Academic, San Diego, Calif., 1987.

Bacmeister, J. T., M. R. Schoeberl, M. E. Summers, J. R. Rosenfield, and X. Zhu, Descent of long-lived trace gases in the winter polar vortex, *J. Geophys. Res.*, *100*, 11,669–11,684, 1995.

Bacmeister, J. T., D. E. Siskind, M. E. Summers, and S. D. Eckermann, Age of air in a zonally averaged two-dimensional model, *J. Geophys. Res.*, *103*, 11,263–11,288, 1998.

Baldwin, M. P., et al., The quasi-biennial oscillation, *Rev. Geophys.*, *39*, 179–229, 2001.

Burrage, M. D., R. A. Vincent, H. G. Mayr, W. R. Skinner, N. F. Arnold, and P. B. Hays, Long-term variability in the equatorial middle atmosphere zonal wind, *J. Geophys. Res.*, *101*, 12,847–12,854, 1996.

Cordero, E. C., and T. R. Nathan, The influence of wave- and zonal mean-ozone feedbacks on the quasi-biennial oscillation, *J. Atmos. Sci.*, *57*, 3426–3442, 2000.

Dunkerton, T. J., On the role of the Kelvin wave in the westerly phase of the semiannual zonal wind oscillation, *J. Atmos. Sci.*, *36*, 32–41, 1979.

Dunkerton, T. J., Nonlinear propagation of zonal winds in an atmosphere with Newtonian cooling and equatorial wavedriving, *J. Atmos. Sci.*, *48*, 236–262, 1991.

Dunkerton, T. J., Inferences about QBO dynamics from the atmospheric "tape recorder" effect, *J. Atmos. Sci.*, *57*, 230–246, 2000.

Dunkerton, T. J., Quasi-biennial and subbiennial variations of stratospheric trace constituents derived from HALOE observations, *J. Atmos. Sci.*, *58*, 7–25, 2001.

Garcia, R. R., Parameterization of planetary wave breaking in the middle atmosphere, *J. Atmos. Sci.*, *48*, 1405–1419, 1991.

Garcia, R. R., F. Stordal, S. Solomon, and J. T. Kiehl, A new numerical model of the middle atmosphere, 1, Dynamics and transport of tropospheric trace gases, *J. Geophys. Res.*, *97*, 12,967–12,991, 1992.

Garcia, R. R., T. J. Dunkerton, R. S. Lieberman, and R. A. Vincent, Climatology of the semiannual oscillation of the tropical middle atmosphere, *J. Geophys. Res.*, *102*, 26,019–26,032, 1997.

Geller, M. A., X. Zhou, and M. Zhang, Simulations of the interannual variability of stratospheric water vapor, *J. Atmos. Sci.*, *59*, 1076–1085, 2002.

Gettleman, A., J. R. Holton, and A. R. Douglass, Simulations of water vapor in the lower stratosphere and upper troposphere, *J. Geophys. Res.*, *105*, 9003–9023, 2000.

Ghil, M., et al., Advanced spectral methods for climatic time series, *Rev. Geophys.*, *40*(1), 1003, doi:10.1029/2000RG000092, 2002.

Gray, L. J., A model study of the influence of the quasi-biennial oscillation on trace gas distributions in the middle and upper stratosphere, *J. Geophys. Res.*, *105*, 4539–4551, 2000.

Gray, L. J., and T. J. Dunkerton, The role of the seasonal cycle in the quasi-biennial oscillation of ozone, *J. Atmos. Sci.*, *47*, 2429–2451, 1990.

Gray, L. J., and J. A. Pyle, A two-dimensional model of the quasi-biennial oscillation of ozone, *J. Atmos. Sci.*, *46*, 203–220, 1989.

Gray, L. J., and J. M. Russell III, Interannual variability of trace gases in the subtropical winter stratosphere, *J. Atmos. Sci.*, *56*, 977–993, 1999.

Hall, T. M., and R. A. Plumb, Age as a diagnostic of stratospheric transport, *J. Geophys. Res.*, *99*, 1059–1079, 1994.

Hall, T. M., D. W. Waugh, K. A. Boering, and R. A. Plumb, Evaluation of transport in stratospheric models, *J. Geophys. Res.*, *104*, 18,815–18,839, 1999.

Holton, J. R., and R. S. Lindzen, An updated theory for the quasi-biennial cycle of the tropical stratosphere, *J. Atmos. Sci.*, *29*, 1076–1080, 1972.

Holton, J. R., et al., Stratosphere–troposphere exchange, *Rev. Geophys.*, *33*, 403–439, 1995.

Huang, T., The impact of solar radiation on the quasi-biennial oscillation of ozone in the tropical stratosphere, *Geophys. Res. Lett.*, *23*, 3211–3214, 1996.

Jackson, D. R., S. J. Driscoll, E. J. Highwood, J. E. Harries, and J. M. Russell, Troposphere to stratosphere transport at low latitudes as studied using HALOE observations of water vapour 1992–1997, *Q. J. R. Meteorol. Soc.*, *124*, 169–192, 1998.

Jones, D. B. A., H. R. Schneider, and M. B. McElroy, Effects of the quasi-biennial oscillation on the zonally averaged transport of tracers, *J. Geophys. Res.*, *103*, 11,235–11,249, 1998.

Kinnersley, J. S., and S. Pawson, The descent rates of the shear zones of the equatorial QBO, *J. Atmos. Sci.*, *53*, 1937–1949, 1996.

Li, D., K. P. Shine, and L. J. Gray, The role of ozone-induced diabatic heating anomalies in the quasi-biennial oscillation, *Q. J. R. Meteorol. Soc.*, *121*, 937–943, 1995.

Lindzen, R. S., and J. R. Holton, A theory of the quasi-biennial oscillation, *J. Atmos. Sci.*, *25*, 1095–1107, 1968.

Mayr, H. G., J. G. Mengel, C. A. Reddy, K. L. Chan, and H. S. Porter, Properties of the QBO and SAO generated by gravity waves, *J. Atmos. Terr. Phys.*, *62*, 1135–1154, 2000.

Mote, P. W., K. H. Rosenlof, M. E. McIntyre, E. S. Carr, J. C. Gille, J. R. Holton, J. S. Kinnersley, H. C. Pumphrey, J. M. Russell, and J. W. Waters, An atmospheric tape recorder: The imprint of tropical tropopause temperatures on stratospheric water vapor, *J. Geophys. Res.*, *101*, 3989–4006, 1996.

Mote, P. W., T. J. Dunkerton, M. E. McIntyre, E. A. Ray, P. H. Haynes, and J. M. Russell III, Vertical velocity, vertical diffusion, and dilution by midlatitude air in the tropical lower stratosphere, *J. Geophys. Res.*, *103*, 8651–8666, 1998.

Naujokat, B., An update of the observed quasi-biennial oscillation of the stratospheric winds over the tropics, *J. Atmos. Sci.*, *43*, 1873–1877, 1986.

Niwano, M., and M. Shiotani, Quasi-biennial oscillation in vertical velocity inferred from trace gas data in the equatorial lower stratosphere, *J. Geophys. Res.*, *106*, 7281–7290, 2001.

Plumb, R. A., and R. C. Bell, Equatorial waves in steady zonal shear flow, *Q. J. R. Meteorol. Soc.*, *108*, 313–334, 1982.

Plumb, R. A., and J. Eluszkiewicz, The Brewer–Dobson circulation: Dynamics of the tropical upwelling, *J. Atmos. Sci.*, *56*, 868–890, 1999.

Randel, W. J., F. Wu, J. M. Russell, A. Roche, and J. W. Waters, Seasonal cycles and QBO variations in stratospheric CH_4 and H_2O observed in UARS HALOE data, *J. Atmos. Sci.*, *55*, 163–185, 1998.

Randel, W. J., F. Wu, R. Swinbank, J. Nash, and A. O'Neill, Global QBO circulation derived from UKMO Stratospheric Analyses, *J. Atmos. Sci.*, *56*, 457–474, 1999.

Randel, W. J., F. Wu, A. Gettleman, J. M. Russell III, J. M. Zawodny, and S. J. Oltmans, Seasonal variation of water vapor in the lower stratosphere observed in Halogen Occultation Experiment Data, *J. Geophys. Res.*, *106*, 14,313–14,325, 2001.

Reed, R. J., A tentative model of the 26-month oscillation in tropical latitudes, *Q. J. R. Meteorol. Soc.*, *90*, 441–466, 1964.

Rosenfield, J. E., M. R. Schoeberl, and M. A. Geller, A computation of the stratospheric diabatic circulation using an accurate radiative transfer model, *J. Atmos. Sci.*, *44*, 859–876, 1987.

Siskind, D. E., On the coupling between middle and upper atmospheric odd nitrogen, *Atmospheric Science Across the Stratopause, Geophys. Monogr. Ser.123*, edited by D. E. Siskind et al., 342 pp., AGU, Washington, D. C., 2000.

Siskind, D. E., J. T. Bacmeister, M. E. Summers, and J. M. Russell III, Two dimensional model calculations of nitric oxide transport in the middle atmosphere and comparison with Halogen Occultation Experiment data, *J. Geophys. Res.*, *102*, 3527–3545, 1997.

Siskind, D. E., S. D. Eckerman, J. P. McCormack, M. J. Alexander, and J. T. Bacmeister, Hemispheric differences in the temperature of the summertime stratosphere and mesosphere, *J. Geophys. Res.*, doi:10.1029/2002JD002095, in press, 2002.

Summers, M. E., D. E. Siskind, J. T. Bacmeister, R. R. Conway, S. E. Zasadil, and D. F. Strobel, Seasonal variation of middle atmospheric CH_4 and H_2O with a new chemical–dynamical model, *J. Geophys. Res.*, *102*, 3503–3526, 1997.

Waugh, D. W., D. B. Considine, and E. L. Fleming, Is upper stratospheric chlorine decreasing as expected?, *Geophys. Res. Lett.*, *28*, 1187–1190, 2001.

Yulaeva, E., J. R. Holton, and J. M. Wallace, On the cause of the annual cycle in the tropical lower stratospheric temperature, *J. Atmos. Sci.*, *51*, 169–174, 1994.

Zhu, X., M. E. Summers, and D. F. Strobel, Calculation of CO_2 15 micron band atmospheric cooling rates by Curtis matrix interpolation of correlated k-coefficients, *J. Geophys. Res.*, *97*, 12,787–12,797, 1992.

J. P. McCormack and D. E. Siskind, E. O. Hulburt Center for Space Research, Naval Research Laboratory, 4555 Overlook Avenue SW, Washington, DC 20375, USA. (mccormack@nrl.navy.mil)